Monthly Notices
of the
ROYAL ASTRONOMICAL SOCIETY

MNRAS **484,** 4507–4528 (2019)
Advance Access publication 2019 January 28

doi:10.1093/mnras/stz241

The Palomar Transient Factory Sky2Night programme

J. van Roestel,[1★] P. J. Groot,[1] T. Kupfer,[2,3,4] K. Verbeek,[1] S. van Velzen,[5] M. Bours,[6] P. Nugent,[7] T. Prince,[4] D. Levitan,[4] S. Nissanke,[1] S. R. Kulkarni[4] and R. R. Laher[8]

[1]*Department of Astrophysics/IMAPP, Radboud University Nijmegen, PO Box 9010, NL-6500 GL, Nijmegen, the Netherlands*
[2]*Kavli Institute for Theoretical Physics, University of California, Santa Barbara, CA 93106, USA*
[3]*Department of Physics, University of California, Santa Barbara, CA 93106, USA*
[4]*Cahill Center for Astronomy and Astrophysics, California Institute of Technology, Pasadena, CA 91125, USA*
[5]*Center of Cosmology and Particle Physics, New York University, New York, NY 10003, USA*
[6]*Instituto de Física y Astronomía, Universidad de Valparaíso, Avenida Gran Bretana 1111, Valparaíso 2360102, Chile*
[7]*Lawrence Berkeley National Laboratory, UC Berkley Department of Astronomy, Berkeley, CA, USA*
[8]*Spitzer Science Center, California Institute of Technology, Pasadena, CA 91125, USA*

Accepted 2019 January 21. Received 2019 January 9; in original form 2018 August 5

ABSTRACT

We present results of the Sky2Night project: a systematic, unbiased search for fast optical transients with the Palomar Transient Factory. We have observed 407deg^2 in *R*-band for eight nights at a cadence of 2 h. During the entire duration of the project, the 4.2 m William Herschel Telescope on La Palma was dedicated to obtaining identification spectra for the detected transients. During the search, we found 12 supernovae, 10 outbursting cataclysmic variables, nine flaring M-stars, three flaring active galactic nuclei, and no extragalactic fast optical transients. Using this systematic survey for transients, we have calculated robust observed rates for the detected types of transients, and upper limits of the rate of extragalactic fast optical transients of $\mathcal{R} < 37 \times 10^{-4}\mathrm{deg}^{-2}\,\mathrm{d}^{-1}$ and $\mathcal{R} < 9.3 \times 10^{-4}\mathrm{deg}^{-2}\,\mathrm{d}^{-1}$ for time-scales of 4 h and 1 d and a limiting magnitude of $R \approx 19.7$. We use the results of this project to determine what kind of and how many astrophysical false positives we can expect when following up gravitational wave detections in search for kilonovae.

Key words: stars: dwarf novae – supernovae: general.

1 INTRODUCTION

Fast optical transients are transients which appear and disappear within 24 h or less. The rate of fast optical transients is not well known (see Fig. 1). The reason why the fast transient sky has not yet been systematically explored is due to technical limitations. To find fast transients, a high cadence is required, which means that area and/or depth need to be sacrificed. For example, a 3-d cadence supernova survey can cover an area 100 times larger than a survey of optical transients with a cadence of 1 h (using the same setup). In addition, follow up of fast optical transients is difficult since it requires rapid detection and identification of the transient and triggering of a follow-up telescope.

For this reason, almost all known extragalactic fast optical transients (time-scales of less than 1 d) have been found as a counterpart of a transient detected at another wavelength where larger solid angle facilities are possible, e.g. X-ray or gamma-ray satellites. The most well studied are gamma-ray burst afterglows: interactions between highly relativistic outflows (jets) and their environment (e.g. Piran 1999). Although they can be bright, because of the low rate ($\approx$1000 yr^{-1} with $R < 20$, Cenko et al. 2015) and, in particular, because of their rapid fading ($\sim$ magnitudes per hour, e.g. Fong et al. 2015; Singer et al. 2015) they are very difficult to find in blind searches. So far, only one[1] GRB afterglow has been found in a blind search: iPTF14yb (Cenko et al. 2015).

In searches for fast extragalactic transients, many Galactic fast optical transients are detected: outbursts of stars in our Galaxy with short ($\sim$1 d) time-scales. These are sometimes considered a 'foreground fog', but they are also interesting to study in their own right. Flaring M-dwarfs are the most common Galactic fast optical transients with typical time-scales of 10-100 min (Hawley et al. 2014; Silverberg et al. 2016) up to 7 h (Kowalski et al. 2010) and outburst magnitudes up to 9 magnitudes in V-band (e.g. Schmidt et al. 2014). Understanding M-flare rates and intensities have recently become important with regards to planetary habitability (e.g. Vida et al. 2017). The other type of common Galactic transients are eruptions in compact binary systems with an accretion disc. The

[1]a strong candidate without a gamma-ray detection is described by Cenko et al. (2013)

★ E-mail: j.vanroestel@astro.ru.nl

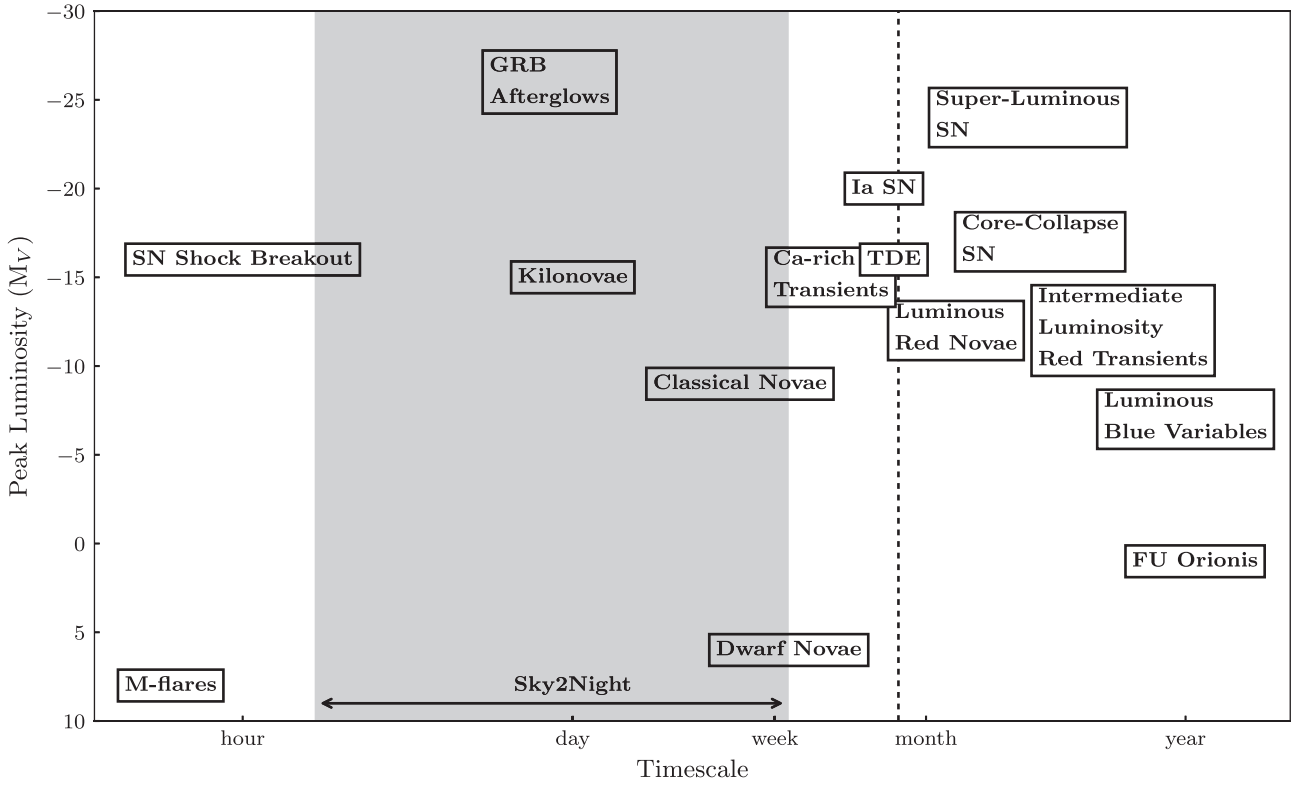

Figure 1. The absolute luminosity versus the typical time-scale of transients. The grey area shows the time-scales which are probed by the Sky2Night project. The dashed line shows the time between the acquisition of the reference images and the end of the survey. This figure is adapted from Kasliwal (2011).

most common are dwarf novae (DN), caused by accretion disc instabilities in systems where a white dwarf accretes mass from a main sequence companion. These outbursts can brighten the system by up to 8 magnitudes (e.g. WZ Sge, Harrison et al. 2004), with short-rise time-scales (∼1 d) and can last for a few days to weeks (Warner 2003).

In 2017, the aLIGO/aVirgo gravitational wave observatories (Acernese et al. 2015; LIGO Scientific Collaboration et al. 2015) detected the first binary neutron star (BNS) merger (Abbott et al. 2017a). Rapid optical follow up of this event resulted in the discovery of the optical counterpart AT 2017gfo (Abbott et al. 2017b,c, see also: Andreoni et al. 2017; Arcavi et al. 2017; Coulter et al. 2017; Cowperthwaite et al. 2017; Díaz et al. 2017; Drout et al. 2017; Evans et al. 2017; Hu et al. 2017; Kasliwal et al. 2017; Pian et al. 2017; Shappee et al. 2017; Smartt et al. 2017; Tanvir et al. 2017; Troja et al. 2017; Utsumi et al. 2017; Valenti et al. 2017; Lipunov et al. 2018; Pozanenko et al. 2018). The optical counterpart, called a kilonova, had been theorized to accompany a BNS merger by Li & Paczyński (1998); Kulkarni (2005); Metzger et al. (2010); Roberts et al. (2011); Barnes & Kasen (2013); Tanaka & Hotokezaka (2013); Metzger & Fernández (2014); Kasen, Fernández & Metzger (2015). AT2017gfo is consistent with the kilonova model predictions: it was fading rapidly ($\Delta r \approx 1.2$ mag d^{-1}), had a peak absolute magnitude of $M_r \approx -16$ mag and displayed rapid reddening (≈ 0.8 mag d^{-1} in $g-r$).

The optical signal can be well modelled using either two or three outflow components. The two-component models are a combination of a rapidly fading 'blue' component, emitted by fast-moving, low-opacity material, and a slower fading 'red' component emitted by slower moving, high-pacity material. Three component models add an additional 'purple' component, with intermediate velocity and opacity. Villar et al. (2017) show that a three-component model is the best explanation for kilonova AT2017gfo. However, we should be aware that future kilonovae can be quite different than AT2017gfo. For example, a lower amount of ejected mass and a different viewing angle results in a kilonovae which is significantly fainter, from $M_R = -16$ down to $M_R = -12$ (e.g. Kasen et al. 2015; Rosswog et al. 2017).

Currently, the aLIGO/aVirgo detectors are being upgraded, increasing the distance (and thus volume) at which they can detect BNS mergers. However, the localization of the events will remain relatively poor (120–180 deg^2, depending on the SNR of the event, Abbott et al. 2016). This means after the detection of a BNS merger, optical telescopes will still have to search a large area to find the faint optical counterpart, $R \approx 19.5$ mag at 200 Mpc if it is similar to AT2017gfo. One of the problems is that in such a large area and magnitude limit, many other (fast) transients will appear which can be confused for a kilonova; a 'needle-in-the-haystack' problem.

In the last decade, there have been a few studies that performed a blind search for fast transients in an attempt to determine the observed rate of fast optical transients. One of the earliest attempts was by Becker et al. (2004). They carried out an unbiased transients search on the data from the Deep Lensing Survey (DLS, Wittman et al. 2002) and found two M-flares and one potential extragalactic transient (OT20030305). However, follow up of the quiescent counterpart by Kulkarni & Rau (2006) shows that OT20030305 is also a flaring M-star. Other searches also found only Galactic transients, mainly cataclysmic variables (CVs) and M-dwarf flares. For example, Rykoff et al. (2005) used the ROTSE-II survey to search for untriggered GRBs but found only six outbursting cataclysmic variables. Rau et al. (2008) performed a high-cadence survey on the Fornax galaxy cluster (cadence 32 min, depth

$B = 22$ mag). They also did not find any extragalactic fast optical transients in their search. The first multicolour search for fast optical transients was performed by Berger et al. (2013), who showed that colours are very useful in identifying the transients. In their search for fast transients, they only found flares on faint M-stars and slow-moving asteroids. More recently, Cowperthwaite et al. (2018) and Utsumi et al. (2018) performed multicolour surveys with the goal to measure the rate of false positives when searching for kilonovae.

In this paper, we present an 8-d unbiased search for all transients in 407 deg^2 of the sky. The search was combined with rapid, unbiased spectroscopic follow-up. To identify the transients, we used the Palomar Transient Factory (PTF) and for immediate (within 24 h spectroscopic follow-up we used the William Herschel Telescope (WHT, Boksenberg 1985). The main goals of the project are to measure the rate of intra-night transients (Galactic and extragalactic) and to determine the expected types of false positives when searching for the optical counterpart of gravitational waves by BNS mergers. The survey design is discussed in Section 2. The execution of the observations and data reduction are described in Section 3. The results: the survey characteristics, an overview of all detected transients, and the observed transient rates are presented in Section 4. We discuss the results in Section 5. The last section summarizes the paper and lists the main conclusions.

2 SURVEY DESIGN

The project consists of two parts: identification of transients with PTF, and rapid spectroscopic classification with the WHT.

To search the sky for transients, PTF used the 48-inch Oschin Schmidt Telescope at Palomar Observatory (P48), equipped with the CFH12K camera. The mosaic camera consists of 11 working CCDs with 4k × 2k pixels each. The system has a pixel scale of 1.01″ pixel^{-1} and a total field of view of 7.26 square degrees (Law et al. 2009; Rau et al. 2009). P48 was available for 8 nights of dark time on 2010 November 1–8 (in MJD range 55501.08–55508.85). We used the standard PTF setup of 60 s exposure times and the $R_{\rm Mould}$ filter (R in the rest of the paper). We chose a target cadence of 2 h and observed the same 59 PTF fields every night (see Table A1 for an overview). The fields are adjacent to each other on the sky and slightly overlapping, so the effective area covered is 407 deg^2. The fields were selected such that they were observable the entire night and are located at an intermediate Galactic latitude ($-45^\circ < b < -25^\circ$), allowing us to study both Galactic and extragalactic transients (see Fig. 1). The ecliptic latitude of the fields is between $-3^\circ < \lambda < 15^\circ$.

To be able to rapidly identify fast transients, PTF used an automated image processing pipeline which does bias and flatfield corrections, source extraction, and image subtraction on all new images (Cao, Nugent & Kasliwal 2016). Reference images of the target fields were obtained 14–16 d before the start of the project. Each reference image was constructed using at least five individual images. The difference images were presented to human scanners to identify transient candidates of interest and reject false positives. The best candidates were marked for follow-up spectroscopy.

We used the 4.2-m William Herschel Telescope (WHT) on La Palma, Spain, to obtain classification spectra of new transients. The WHT was dedicated for this purpose for 7 nights starting after the first night of PTF observations (MJD 55501.75). The instrument used to observe the transients was ACAM (Benn, Dee & Agócs 2008). ACAM is both an imager and low-resolution spectrograph ($R \approx 500$, 4000–9000 Å) and is therefore ideally suited for rapid transient identification. We first observed the candidate transients with ACAM in imaging mode to confirm if they are real and to determine the brightness, followed by an identification spectrum.

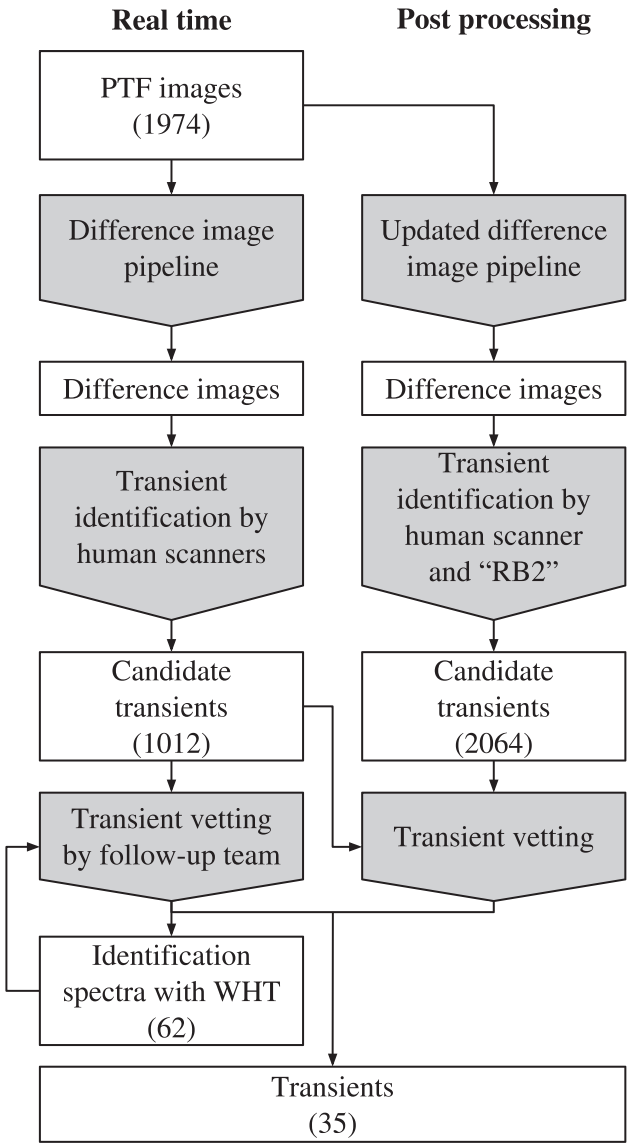

Figure 2. The Sky2Night data analysis and transient detection procedure. The left column shows the real-time analysis of the data, the right column shows the re-analysis of the data. White boxes show data products, within brackets the number of items, grey boxes indicate operations/filters which are applied to the data.

3 OBSERVATIONS

During the project, the weather at the P48 was mostly good. Fifteen per cent of the time was lost due to bad weather, mostly during nights 2, 7, and 8. The seeing was typically 2.5″, but it was highly variable and regularly increased up to 4″ (Table A2). A total of 1974 exposures were obtained, with a median of 5 exposures per field per night. Fewer observations were obtained during nights 2, 7, and 8; with a median of 3, 3, and 2 observations per field. A full overview of all PTF observations can be found in Table A3.

Fig. 2 shows a schematic overview of the data reduction and transient detection process. The new images were processed and

Table 1. The different types of transient candidates found in the real-time search.

Type	#
Point-source counterpart	
- Star	873
- QSO	15
- Faint star ($R \gtrsim 20.5$)	3
Galaxy counterpart	
- Nuclear	48
- Near galaxy	12
Artefact	26
Moving object	35
Total	1012

difference images were created by the PTF pipeline as quickly as possible (see Section 2). This ranged from half an hour to a few hours after the observation because the image processing pipeline could not keep up with the flow of incoming images. As soon as the difference images were available, they were analysed by multiple human scanners to identify new transients. Identifying the real transients on the difference images was not trivial since the difference images contained many artefacts (e.g. slight misalignments of the images, bad pixels). To reduce the time spend on visual inspection of candidates, we only inspected candidate transients which had two or more detections. This was done to get rid of asteroids but also filtered out some of the artefacts. In addition, the human scanners were assisted by a machine learning algorithm to get rid of the most obvious false positives (a rudimentary version of the 'RealBogus' pipeline, see Bloom et al. 2012, Cao et al. 2016, and also Smith et al. 2011). A total of 1012 candidate transients were judged by the human scanners to be potentially real, and these were passed on for further inspection by the follow-up team at the WHT.

The 1012 candidate transients were more carefully vetted by the follow-up team by inspecting the images obtained by PTF and, if available, SDSS images (Abazajian et al. 2009). In addition, we checked if the target corresponded to a known object in SIMBAD data base.[2] An overview of the different kinds of transient candidates is given in Table 1. The bulk of the potential transients were associated with a known point-like source. The majority (873) of these were either due to bad subtraction of a star or low amplitude variability of a star. Besides variable stars, there were also 15 QSOs which brightened significantly during the project. We found three transient candidates without a counterpart in the PTF images, but for which a point-source was detected in the SDSS images. For all three, the SDSS and Pan-STARRS catalogues indicate that they are pointsources. A number of potential transients (60) were found near a galaxy. The majority of these (48) were at the core of the galaxy, and it is difficult to determine if this is a bad subtraction, AGN activity, or a supernova in the core of a galaxy. Five of these could be matched to a known AGN. Experience with other PTF data indicates that the remaining nuclear transients are likely bad subtractions or AGN. The 12 remaining transients with a nearby galaxy were strong supernova candidates. A few objects (35) were initially flagged as transients but were later identified as moving objects. In addition, 26 candidates were caused by artefacts (bad pixels, very bright stars, and 'ghosts').

The PTF imaging data was thoroughly re-analysed in 2014 to make sure no transients were missed during the initial search (the right column in Fig. 2). The images were reprocessed using an improved version of the image processing pipeline. New difference images were made. All sources present on the new difference images were analysed using the 'RealBogus2' pipeline (Brink et al. 2013; Cao et al. 2016). We used a lower than normal threshold value of 0.3, compared to the 0.53 advised in the paper. This lower threshold corresponds to a missed detection rate of 5 per cent (compared to 10 per cent for a threshold of 0.53). This second search resulted in 2064 candidates transients, of which 105 overlap with the initial sample of 1012 sources. All these transient candidates were vetted using PTF, SDSS, and Pan-STARRS (Chambers et al. 2016) images and CRTS light curves (Drake et al. 2009) and also using the SIMBAD data base. This re-analysis recovered all real transients identified by the human scanners during the Sky2Night run. However, we also identified two faint supernovae and five flaring M-stars in the overlapping sample of transients. In addition, one new flaring M-star was found that was missed entirely during the initial search.

The most promising candidate transients found during the real-time search, typically transient candidates which were bright or were rapidly getting brighter, or were located off-centre from a galaxy, were observed with the WHT telescope. The results are shown in Table A4. The majority of the supernovae (8) are of type Ia. Since we obtained both a spectrum and an 8-d light curve, there is little uncertainty in the classification. The subtypes are more difficult to determine, but all except two, appear to be normal type Ia supernovae (for an overview of Ia subtypes, see, for example, Taubenberger 2017). PTF10aaiw, for which we have two spectra, is a '91T'-like supernova (Filippenko et al. 1992b) according to the cross-correlation with template spectra. The spectra of PTF10aaiw show a shallow II 6355 Å absorption line and deep Fe III absorption features, which are the main features discriminating '91T"-type supernovae from normal SNIa supernovae. In addition, the absolute peak magnitude as determined from the light curve fit, $M_B \approx -19.5$, is consistent with being a '91T"-type supernova. PTF10zej could be a '91bg"-type supernova (Filippenko et al. 1992a); the obtained spectra match almost equally well with '91bg"-templates and normal Ia-template spectra. The estimated absolute magnitude is only $M_B \approx -18.0$, which puts it at the boundary between normal Ia supernova and '91bg'-type supernovae. With the available data, we cannot make a certain sub-classification of the subtype of PTF10zej. The results are shown in Table A4. The majority of the supernovae (8) are of type Ia. Since we obtained both a spectrum and an 8-d light curve, there is little uncertainty in the classification. The subtypes are more difficult to determine, but all except two, appear to be normal type Ia supernovae (for an overview of Ia subtypes, see, for example, Taubenberger 2017). PTF10aaiw, for which we have two spectra, is a '91T"-like supernova (Filippenko et al. 1992b) according to the cross-correlation with template spectra. The spectra of PTF10aaiw show a shallow Si II 6355 Å absorption line and deep Fe III absorption features, which are the main features discriminating '91T"-type supernovae from normal SNIa supernovae. In addition, the absolute peak magnitude as determined from the light-curve fit, $M_B \approx -19.5$, is consistent with being a '91T'-type supernova. PTF10zej could be a '91bg'-type supernova (Filippenko et al. 1992a); the obtained spectra match almost equally well with '91bg'-templates and normal Ia-template spectra. The estimated absolute magnitude is only $M_B \approx -18.0$, which puts it at the boundary between normal Ia supernova and '91bg'-type supernovae. With the available data, we cannot make a certain sub-classification of the subtype of PTF10zej. During the spectroscopic follow-up, the weather was variable. Most nights were clear, but

[2] http://simbad.u-strasbg.fr/simbad/

during nights 2 and 3 time was lost due to passing clouds. Although night 7 was clear, about half the time was lost due to high humidity. The seeing during the nights varied between 0.8″and 4″. Table A2 shows an overview of the weather conditions at the WHT. A total of 62 transient candidates were observed. Exposure times of the spectra range between 300 s and 1200 s. For calibration, either standard star SP2157+261 or SP0804 + 751 were observed at the beginning or end of the night. A quick reduction of the spectra was performed within 24 h in order to identify any events which might need additional follow-up. The data were later reduced using standard procedures using IRAF. For some transients, spectra were obtained with other telescopes as part of the PTF collaboration and were also used in the identification of transients (see also Table 2). All these spectra (including header information) are available on Wiserep[3] (Yaron & Gal-Yam 2012).

4 RESULTS

4.1 Survey characteristics

An overview of the most important metrics of the survey is given in Fig. 3. The time between observations, generally referred to as cadence, is given in the top left-hand panel in Fig. 3. The median time between observations is 2.0 h within a night and almost all fields have been revisited within 3 h. There is also a longer delay of about 16.8 h between revisits, which is due to the day–night cycle.

The limiting magnitude of the observations are shown in the top right-hand panel. We empirically measure the limiting magnitude by calculating the 95th percentile magnitude of all sources detected in the image. The source detection by PTF is performed with SEXTRACTOR (Bertin & Arnouts 1996) with a detection threshold of four standard deviations above the background noise. The median limiting magnitude of all observations is $R = 20.18$ mag, with 95 per cent of the observations in the range of $R = 18.92$ mag and $R = 20.70$ mag (top right -hand panel in Fig. 3). The figure also shows the distribution of the limiting magnitude of the deepest image per night (median $R = 20.41$ mag) and the second deepest image per night (median $R = 20.27$ mag), which is the relevant measure for transients which are visible for longer than 1 d. In addition, the distribution for individual nights is plotted, which shows that the nights are comparable, except for nights 2 and 8, due to clouds. Note that the limiting magnitudes are not randomly distributed in each night, but vary as a function of time in the night (see Fig. A1). This is caused by the airmass-related extinction as the fields are tracked from horizon to horizon. At the beginning of the night, the limiting magnitude is about $R \approx 20.0$ mag per exposure and increases to $R \approx 20.4$ mag during the middle of the night, and then decreases again to $R \approx 20.0$ mag towards the end of the night. A few spikes can be seen in the limiting magnitudes as a function of time which are caused by passing clouds.

In order to calculate an observed rate of transients, we need to determine how much area we have effectively monitored and for how long: the areal exposure $E_A(\tau)$ (units: deg^2 d), which is a function of how long a transient is visible (τ). To calculate the areal exposure for Sky2Night, we test if a transient (visible for a set duration τ) would have been detected at least twice in our survey. The result for transients visible for $\tau = 4$ h and $\tau = 1$ d is shown as the shaded area in the mid-left panel in Fig. 3. The total areal exposure for a given visibility time can be calculated by integrating over time (i.e. the area of the shaded surface in the mid-left panel). The areal exposure as a function of visibility time (τ) is shown in the mid-right panel. Here, we also show the areal exposure if we take the limiting magnitude of the images into account. The bottom panel shows the same information in a different way: the fraction of areal exposure that is available as a function of magnitude. This shows that there is almost no loss of areal exposure for long time-scale transient before magnitude $R = 19.5$, but for the short time-scale transients, the areal exposure already starts to decrease at $R \approx 18$. This shows that the areal exposure on short time-scales is more sensitive to low limiting observations than the longer time-scales. In the rest of the paper, we will use the areal exposure assuming that all images can be used (the black line in the mid-right panel, 1 in the bottom panel) to calculate the observed rate of transients.

4.2 Transients

All transients that were identified as real are listed in Table 2 and shown in Fig. 4. We found a total of 12 supernovae, 10 cataclysmic variables, 9 flaring M-stars, and 3 flaring AGN. We will discuss each class separately in the following sections.

4.2.1 Supernovae

We found a total of 12 supernovae in the Sky2Night area. They are listed in Table 2 and the light curves and spectra are shown in Fig. A2. For most of the supernovae, we have at least eight nights of photometry. For 10 supernovae, an ACAM spectrum is available. For some supernovae, additional spectra are available that were obtained as part of other programs in the PTF collaboration. For the two faint supernovae that were not found in the real-time search (PTF10zqz and PTF10zxs), no spectra are available.

To determine the type and sub-type of the supernovae, we use SNID (Blondin & Tonry 2007) to cross-correlate the spectra with supernova template spectra. If possible, we determine the redshift from the host galaxy or use narrow emission lines in the supernova spectrum. If this is not possible, we use the average redshift from the SNID cross-correlation. For the supernovae without a spectrum, we use the SDSS photometric redshift. To determine the age of the supernovae, we fit a supernova light-curve template to the PTF difference imaging photometry using the python package SNCOSMO (Barbary 2014). For the Ia supernovae, we use the template light curves from Hsiao et al. (2007) and for the core-collapse supernovae we use the templates from Gilliland, Nugent & Phillips (1999).[4]

The results are shown in Table A4. The majority of the supernovae (8) are of type Ia. Since we obtained both a spectrum and an 8-d light curve, there is little uncertainty in the classification. The subtypes are more difficult to determine, but all except two, appear to be normal type Ia supernovae (for an overview of Ia subtypes, see, for example, Taubenberger 2017). PTF10aaiw, for which we have two spectra, is a '91T'-like ,supernova (Filippenko et al. 1992b) according to the cross-correlation with template spectra. The spectra of PTF10aaiw show a shallow Si II 6355 Å absorption line and deep Fe III absorption features, which are the main features discriminating '91T'-type supernovae from normal SNIa supernovae. In addition, the absolute peak magnitude as determined from the light-curve fit, $M_B \approx -19.5$, is consistent with being a '91T'-type supernova. PTF10zej could be a '91bg'-type supernova

[3] https://wiserep.weizmann.ac.il/

[4] 'Nugent' supernovae templates available at https://c3.lbl.gov/nugent/nugent_templates.html

Table 2. Overview of all transients found, sorted by discovery date. Shaded rows indicate extragalactic transients. The first detection column lists the time when the transient was first detected on an image. The discovery column shows the time when the transient was identified by the human scanners. The counterpart column lists the magnitude of the quiescent counterpart with *R* indicating the PTF *R* magnitude, and *r* the SDSS or Pan-STARRS *r* magnitude (the faintest of the two) for point sources. That the counterparts are point sources has been determined from both the SDSS and Pan-STARRS catalogues. The spectrum column lists the sources of the spectra; 'ACAM': observations with ACAM at the WHT (see Section 2), 'R.C. Spec': R.C. Spectrograph at the 4-m Mayall telescope at KPNO (Arcavi et al. 2010), 'Kast': Kast spectrograph at the 3 m Shane telescope at Lick Observatory, 'LRIS': LRIS at Keck-1 (Oke et al. 1995). 'DBSP': DBSP at the Hale telescope (P200, Oke & Gunn 1982).

Name PTF ...	Ra (°)	Dec (°)	First detection (MJD-55501)	Discovery (MJD-55501)	Type	Counterpart	spectrum
10vey	21.734133	24.188559	–46.5	–46.5	CV	$R = 19.37$	
10aaqh	58.242271	21.424262	–3.76	–1.78	M-flare	$R = 16.50$	ACAM
10zbk[a]	37.393757	22.333575	–1.76	–1.72	SN/Ia	galaxy	R.C. Spec, Kast
10zcd[b]	17.137369	16.502957	–1.76	0.13	SN/Ia	galaxy	ACAM, R.C. Spec
10zej[c, d]	31.760443	20.853715	0.1	0.19	SN/Ia-'91bg"?	galaxy	ACAM
10zeb[e]	26.82027	15.82885	–1.82	0.22	QSO/BL Lac	$r = 19.20$	
10zhi[b]	23.101224	21.455835	0.19	0.27	SN/Ia	galaxy	R.C. Spec
10zfe	30.067678	23.926279	0.34	0.34	M-flare	$R = 18.15$	
10zdq	27.478711	21.033048	0.19	0.36	SN/Ia	galaxy	ACAM
10zdi[f]	31.639451	20.952067	0.1	0.44	CV	$R = 18.44$	ACAM
10zdk[g]	33.530525	23.630602	0.12	0.46	SN/Ia	galaxy	ACAM, R.C. Spec, Kast, LRIS
10zqz	25.085293	19.205094	0.60	0.86	SN	galaxy	
10aacy	27.623838	16.107371	1.17	1.17	M-flare	$R = 16.37$	ACAM
10aadb[h]	35.64689	25.137566	-5.6	1.20	AGN	galaxy	ACAM, DBSP
10zig[i]	22.159879	18.760014	1.31	1.31	CV	$R = 18.22$	
10zix[j]	32.792509	17.273396	1.16	1.33	CV	$R = 19.61$	ACAM
10zxs	37.87864	20.461258	0.20	1.89	SN	galaxy	
10aaop	33.024992	25.166939	1.1	2.18	M-flare	$R = 19.51$	
10aaes[k]	31.791567	16.211025	-19.81	2.20	SN/IIn	galaxy	ACAM
10aaom	54.314202	15.914879	2.24	2.25	M-flare	$R = 18.58$	
10aaho	32.755376	15.785523	0.14	2.27	SN/IIP	galaxy	ACAM, LRIS
10aaey	39.654895	22.056594	0.29	2.31	SN/Ia	galaxy	LRIS
10aafc[l]	51.512414	25.425869	2.33	2.40	CV	$r = 20.17$	ACAM
10aagv	57.774944	21.256824	3.34	3.34	M-flare	$R = 18.34$	
10aajr[m]	33.219913	22.748068	0.26	4.10	QSO/BL lac	$r = 17.83$	
10aaiw[a]	17.338134	15.735881	-2.71	4.13	SN/Ia-'99T"	galaxy	ACAM, KAST
10aakm	51.319163	22.735708	0.14	4.51	M-flare	$R = 15.89$	ACAM
10aaqc[i]	38.260974	18.806173	6.28	6.28	CV	$r = 22.03$	ACAM
10aarq	28.098845	25.613108	6.34	6.34	M-flare	$R = 20.68$	
10aaqt[i]	23.952331	24.400854	6.24	6.40	CV	$r = 23.02$	
10aaqj	50.600737	25.309258	5.33	6.42	CV	$R = 20.16$	ACAM
10aaqb[i]	59.774695	17.842959	6.38	6.46	CV	$R = 18.00$	ACAM
10aaqu[i]	53.982354	19.188484	6.36	6.52	CV	$R = 20.34$	
1401fi	22.82068	26.1559	1.29	>8	M-flare	$r = 21.37$	

Note: The superscript above the name refers to one of the following papers: *a*: Pan et al. (2014), *b*: Arcavi et al. (2010), *c*: Drake et al. (2010a), *d*: Drake et al. (2010b), *e*: D'Abrusco et al. (2014), *f*: Szkody et al. (2014), *g*: Maguire et al. (2012), *h*: Paturel et al. (2003), *i*: Drake et al. (2014), *j*: Kato et al. (2009), *k*: Ackermann et al. (2015), *l*: Oliveira et al. (2017), *m*: Mickaelian et al. (2006).

(Filippenko et al. 1992a); the obtained spectra match almost equally well with '91bg'-templates and normal Ia-template spectra. The estimated absolute magnitude is only $M_B \approx -18.0$, which puts it at the boundary between normal Ia supernova and '91bg'-type supernovae. With the available data, we cannot make a certain sub-classification of the subtype of PTF10zej.

PTF10aaho and PTF10aaes, are core-collapse supernovae. PTF10aaho is a supernova that exploded a few days before the start of the program in a faint, unresolved galaxy ($SDSS_r = 21.36$ mag). The light curve shows a rapid rise during the Sky2Night project, and PTF kept observing the field containing this supernova for a long time. The light curve indicates that this is a normal-type IIP supernova (e.g. Filippenko 1997).

PTF10aaes is likely a core-collapse supernova that occurred off-centre (2.4″ distance) in an elliptical galaxy. The spectrum best matches to that of type-II SN templates of 80 d or older. The lack of any significant trend in the 8-d light curve and the faint absolute magnitude ($M_B = -15.8 \pm 0.5$) also indicate that this is most likely an old supernova. However, if PTF10aaes is indeed an old supernova, we should have detected it in the reference images (taken 15 d before the start of the Sky2Night project) and should not have shown up in the difference images. A visual inspection shows a detection in only one out of the five individual images used to make the reference image. One possibility is that the supernova re-brightened slightly since the reference images were taken, and therefore does appear in the difference images.

We have been unable to identify two supernovae, PTF10zqz and PTF10zxs. They are transients that appeared close to a galaxy (but not in the nucleus of the galaxy). No spectrum is available for PTF10zqz and PTF10zxs, and the light curve does not show any significant evolution over the 8 d of data. With this information, it is not possible to classify these two supernovae.

We also found one false positive supernova, PTF10zfi, which turned out to be a processing artefact. It appeared close to a galaxy,

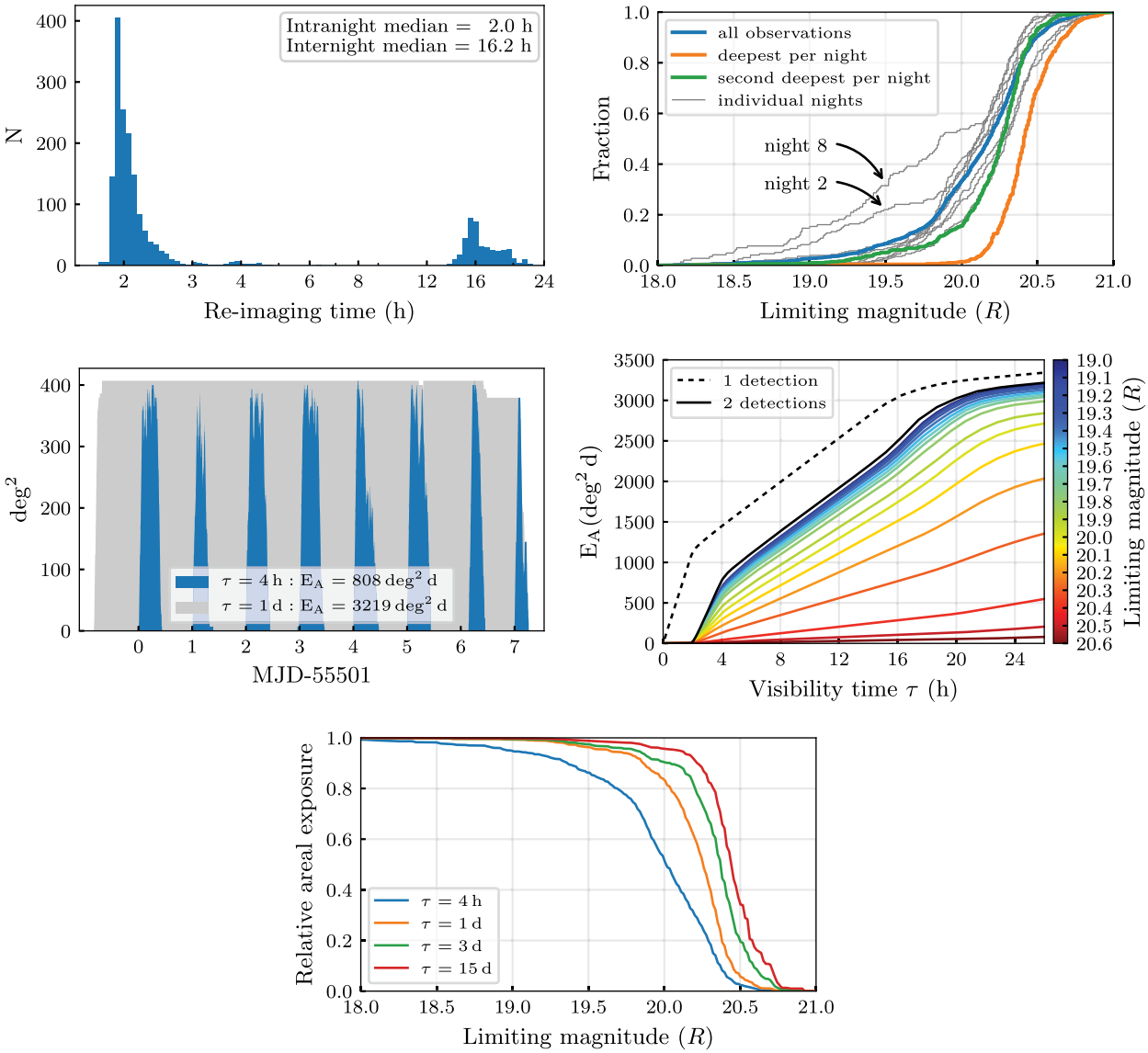

Figure 3. The survey characteristics. (*top-left*) The distribution of time between observations for all fields. (*top-right*) The cumulative histogram of the limiting magnitudes of all observations. (*mid-left*) The number of square degrees in which we are able to find transients with two detections as a function of time. The area under the curve is the areal exposure (E_A). (*mid-right*) The areal exposure (E_A) as function of visibility time (τ). The black line is the areal exposure if all observations are used, while the coloured lines show the areal exposure if observations that reach a certain limiting magnitude are used. (*bottom*) The fraction of the total areal exposure (the black line in the mid-right panel) as function of magnitude for different visibility times.

which is why it was initially confused for a supernova. Two ACAM spectra were obtained of the host galaxy but did not show any sign of a supernova. Re-analysis of the imaging data with forced photometry does not show the transient any more.

4.2.2 *Outbursting Cataclysmic Variables*

We found a total of 10 outbursting CVs in the Sky2Night survey area, see Table A5 and Fig. A3. Out of these systems, five were found by the human scanners during the Sky2Night project and for these five we obtained an ACAM spectrum. We confirmed that these objects are CVs by their spectra which show Balmer emission lines at a redshift of zero. For the remaining systems, we confirmed the CV nature by inspecting their CRTS light curves, which show many eruptions over the 10 + year baseline. Dwarf nova outbursts are the most common type of large amplitude optical variation in CVs, and the majority of CVs we found feature dwarf nova outbursts. The amplitude of the outbursts are typically $R = 1 - 5$ mag and last approximately 4–6 d. Transients PTF10vey, PTF10zdi, PTF10zix, PTF10aafc, and PTF10aaqu are typical examples of dwarf novae outbursts. PTF10aaqb shows an outburst amplitude of only 1.2 magnitudes. However, CRTS archival data show many dwarf nova outbursts with an amplitude of typically 2 magnitudes. We, therefore, conclude that PTF10aaqb is also a dwarf nova outburst.

Transients PTF10aaqc and PTF10aaqt have no counterpart in the PTF images. However, deeper SDSS images and Pan-STARRS images both show a faint, unresolved object. Both transients appeared at the end of the project so the light curve only spans a

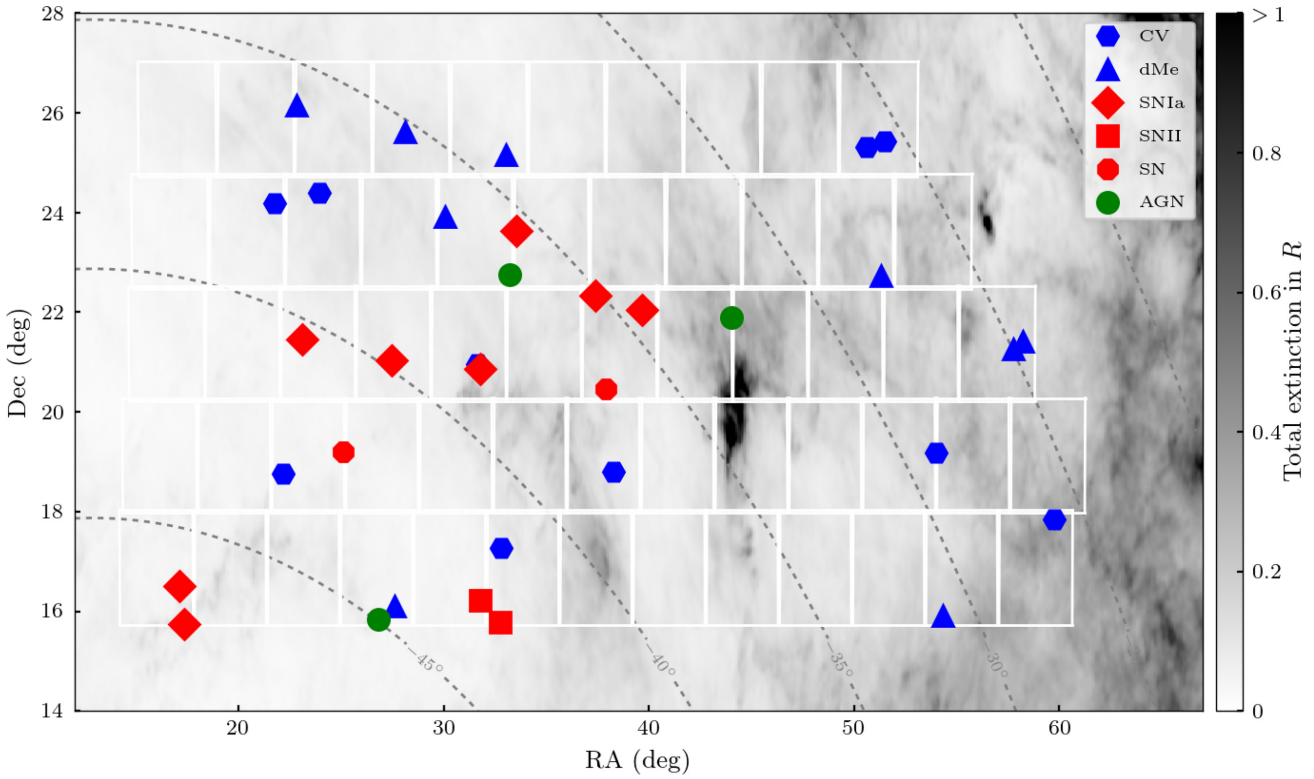

Figure 4. The observed area and all transients found during the project. The white rectangles indicate the 59 PTF fields. The dashed lines indicate different Galactic latitudes. The grey background indicates the total amount of Galactic extinction (Schlegel, Finkbeiner & Davis 1998).

few days and no spectra are available. Both transients are repeating; both in PTF data obtained years later and in CRTS data multiple outbursts of a few days duration can be seen for both objects. We, therefore, also classify PTF10aaqc and PTF10aaqt as dwarf novae.

Transient PTF10zig was in outburst long enough for it to be detected both in the reference image and during the survey. The PTF light curve shows rapid variability ($\sim$ hours) of $\sim$1.5 magnitudes. The few observations were taken before the start of the Sky2Night project hint that this system was already in outburst for 20 d, and possibly 80 d. The CRTS light curve, taken around the same time as the Sky2Night survey, also shows rapid variability of $\sim$1.5 magnitudes. Observations taken by CRTS years earlier and later only detected the source at $\sim$21 mag. The SDSS image also shows a faint source with a colour of $g - r \approx 0.3$ with $r = 21.55$. In addition, an SDSS spectrum is available which shows many Balmer emission lines and also the He I emission line at 5875 Å which confirms the CV nature of the object. However, the light curve does not resemble that of a typical CV with dwarf nova outbursts. The PTF observations could be taken while it was in a super-outburst; long outbursts that can last months and can feature strong variability (e.g. Osaki & Kato 2013). If, indeed, the Sky2Night light curve is part of a long-duration superoutburst, PTF10zig can be classified as an SU UMa or WZ Sge subtype of dwarf nova CVs.

PTF10aaqj showed a slow brightening of about 1 magnitude during the Sky2Night project and was therefore saved as a candidate. The ACAM spectrum feature Balmer emission lines ($z = 0$) and confirms that this is a CV. The CRTS light curve shows non-periodic optical variability but with no clear outbursts. These characteristics match those of AM Her type CVs (Warner 2003).

4.2.3 *Flaring M-stars*

A total of nine flaring stars were identified in the Sky2Night data, see Fig. A4. All except PTFS1401fi were identified as candidate transients, and a spectrum was obtained for three of the objects. The quiescent counterparts of the flaring objects were also detected in PTF reference images, ranging from $R = 16$ mag to $R \approx 21$ mag. We use Pan-STARRS colours to determine the spectral type of the M-dwarfs, following the classification of Best et al. (2018), see Table A6 and Fig. 6. This shows that the majority of the flaring objects are of spectral type M4–M5. Two of the flaring stars were significantly redder and have later spectral types of M6 and M7.

We fit a simple outburst model (instant rise, exponential decay in flux) to the light curves to determine the outburst properties, such as flare magnitude and decay time scale, see Table A6. Here, we have assumed that the highest detected magnitude corresponds to the observed peak magnitude, the most conservative approach. We calculated the energy emitted per flare in the R-band by first measuring the equivalent duration of the flare (Gershberg 1972), and then calculate the absolute energy in the flare by using the absolute magnitudes of M-stars from Pecaut & Mamajek (2013).

The flare time-scales are typically within 0.5 and 2 h, with one longer flare with a time-scale of almost 5 h. The observed flare magnitudes are typically between 0.6 and 1.5 magnitudes, but three flares are significantly stronger, with the strongest flare of 3.5 magnitudes.

4.2.4 AGN activity

Three promising transient candidates were followed up with the WHT but were identified as an AGN. Their light curves and spectra are shown in Fig. A5.

PTF10aadb is a transient at the core of a face-on SAa spiral galaxy ($z \approx 0.062$, Huchra et al. 2012). The light curve during the Sky2Night project has an average of $R \approx 19.5$ mag and does not show a significant trend. The initial spectrum showed what seemed to be a weak Hα P-Cygni profile, and the object was initially identified as a type IIn supernova. However, there is evidence that the core of the galaxy is an AGN. First, a radio source has been detected in the NVSS survey (Condon et al. 1998). Second, observations by PTF three years after the Sky2Night project also show another brightening of the core of this galaxy, now up to $R \approx 18.8$ mag. This makes it more plausible that the transient seen during Sky2Night is due to AGN activity. A spectrum obtained 25 d after the first spectrum shows a huge increase in $H\alpha$ emission and that the O-III lines (4959 and 5007Å) disappeared. In addition, the AGN became significantly brighter at the long wavelengths (>7000 Å). The strong increase of $H\,\alpha$ emission is a typical characteristic of changing look AGN (e.g. Gezari et al. 2017).

PTF10zeb and PTF10aajr both appear as unresolved sources which rapidly became brighter. For PTF10aajr a spectrum was obtained with ACAM. The spectrum shows a blue continuum without any prominent features. Both sources are known radio and X-ray sources and classified as BL Lac-type objects (Mickaelian et al. 2006; D'Abrusco et al. 2014), which agrees with our observations.

4.3 Observed transient rates

The observed rate of transients is calculated as follows:

$$\mathcal{R} = \frac{N}{\epsilon^2 E_A(\tau)}\ (\mathrm{deg}^{-2}\,\mathrm{d}^{-1}) \qquad (1)$$

with N the number of transients, ε the detection efficiency per image, and E_A the effective exposure (see Section 3). Since N is a small number, we use Poisson statistics to calculate the uncertainty (e.g. Gehrels 1986).

We used a simple estimate for the detection efficiency: all transients brighter than the detection limit are recovered ($\varepsilon = 1$) and those fainter than the detection limit are not ($\varepsilon = 0$). The detection efficiency (ε) occurs in the equation squared because we required a transient to be detected in two images. The efficiency is difficult to estimate and is a function of the magnitude, the background (e.g. a galaxy), and the subjective nature of human scanners. We tried to be as complete as possible by saving candidate transients when in doubt. However, the efficiency will always gradually decrease as the brightness approaches the detection limit. Frohmaier et al. (2017) performed a detailed test of the recovery rate as a function of limiting magnitude, brightness of the transient, seeing, angular distance to the nearest galaxy and other parameters. Such a level of detail is not needed in this work, since the Poisson uncertainty dominates the rates and is of the order of 20 per cent or more. We note that Frohmaier et al. (2017) found a maximum recovery efficiency of 97 per cent. In the calculation of the rates, we will assume $\varepsilon = 1$ for transient brighter than the magnitude limit. This should be kept in mind when interpreting the results: if the real efficiency is lower than 1, the real observed transient rates will be slightly higher than reported in this work.

The effective exposure (E_A) depends on the visibility time of the transient, as can be seen in Fig. Fig. 3. We, therefore, need to estimate how long a transient would have been visible during the project. We then use the areal exposure assuming that the transients could have been detected in all images (the black line in the bottom-left panel in Fig. 3). For supernovae, we assume that they are all visible for longer than 15 d. This maximum results from the requirement of a non-detection in the reference images obtained 15 d before the start of the project. For the dwarf novae and BL Lac flares we estimate the visibility time by eye from the light curves, ranging between 3–5 d. For the M-dwarf flares, we have used the fitted curve to estimate the visibility time, which are typically detectable as transient for 3-6 h. We assume an uncertainty on our estimates of the visibility time (τ) 10 per cent (lognormal distributed).

Table 3. The observed rate of transients for the Sky2Night project. The uncertainties indicate the 95 per cent confidence interval. Upper limits for fast optical transients are 95 per cent confidence upper limits. These limits assume a detection efficiency of $\varepsilon = 1$ (see equation (1)) and assume that transients could have been detected in all of the images.

Type	N	$\mathcal{R}$ (10^{-4} deg^{-2} d^{-1})
Supernova - Ia	8	$10.0^{+8.2}_{-5.3}$
Supernova - CC	1	$2.0^{+4.4}_{-1.6}$
CV - DN	5	$12.8^{+13.6}_{-7.9}$
CV - DN - $R > 20.5$ mag	2	$6.0^{+10.3}_{-4.6}$
M-flares	9	118^{+94}_{-58}
M-flares - $R > 20.5$ mag	2	35^{+64}_{-26}
BL Lac flares	2	$6.7^{+11.6}_{-5.0}$
FOTs (4 h)	0	<37
FOTs (1 d)	0	< 9.3

We calculate the observed rate and uncertainty for each type of transient by numerically combining the Poisson distribution for N, with the distribution we calculated for E_A. The final values are shown in Table 3 with the uncertainties indicating the 95 per cent confidence interval. In addition, we calculate an upper limit for transients visible for 4 h and 1 d. We use the 95 percentile upper limit, which corresponds approximately to three detections (Gehrels 1986).

5 DISCUSSION

5.1 Expected number of transients

5.1.1 Supernovae

The expected number of supernovae Ia in the survey are easy to determine since their light curves are very uniform and the volumetric rate for Ia supernovae is well-known (e.g. Graur et al. 2014). In addition, they can be assumed to be uniformly distributed across the sky. We use SNCOSMO to simulate a large number of supernova Ia light curves of uniformly distributed supernovae (in co-moving volume). We use SALT2 supernova light-curve templates (Guy et al. 2007) with parameters and host galaxy extinction parameters according to Mandel et al. (2017). We also take into account Galactic extinction (Schlegel et al. 1998). We simulate our survey by checking if the supernovae are in the Sky2night field and if it is above the detection limit during the survey and not detected in the reference image. For a limiting magnitude of $R = 20.21$ mag (the magnitude at which the fractional areal exposure is 90 per cent, see the bottom panel of Fig. 3) and volumetric rate of (Graur et al. 2014), we would expect to find 13.4 supernovae during our project, marginally consistent with eight confirmed detections taking into

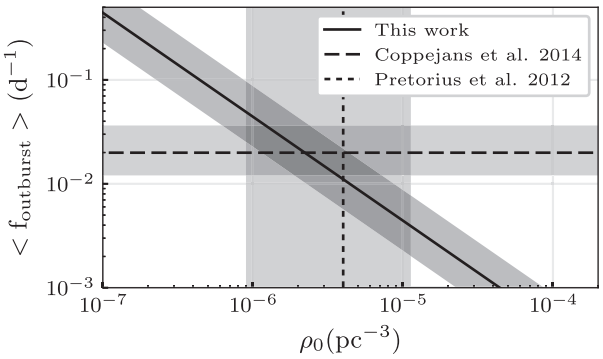

Figure 5. The CV space density versus the average dwarf nova outburst frequency. The dwarf nova volumetric rate we derived in this paper is shown as the diagonal line in the figure. The vertical line shows the space density as measured by Pretorius & Knigge (2012) and the horizontal line shows the average outburst frequency calculated from the dwarf nova sample by Coppejans et al. (2014). The shaded regions indicate a 95 per cent confidence interval.

account Poisson uncertainty. Or, the other way around, we find a volumetric rate of . This suggests that we have missed some supernovae in our search or the effective magnitude limit was about $R \approx 19.8$ mag. Adams et al. (2018), who also used PTF data, also found that the efficiency started to drop of about 0.5 magnitudes above the detection limit. This could be explained due to the fact that Ia supernovae occur in galaxies, which makes their detection more difficult. We compare the relative number of different types of supernovae to the fraction of supernovae found by the Lick Supernova search (Li et al. 2011). They find that 74 per cent of their supernovae are of type Ia, with 17 per cent of type II and 9 per cent type Ibc. Our results are consistent with this result: with 8 out of 9 identified supernovae are of type Ia (we do not count PTF10aaes, as it is an old supernova). The distribution of Ia subtypes is also in agreement with the ratios found in the Lick Supernova search. With 8 detected Ia supernovae, the expectation value for '99T" and '91bg" types is both one, which is what we have found.

5.1.2 *Dwarf novae*

We simulate the number of dwarf novae outbursts which we expect given the CV space density and outburst frequency. We use a simple Galaxy model with a thin and thick disk. We assume disks with an exponentially decreasing density profile with scale heights of 200 per cent and 1000 per cent and a Galaxy scale radius of 3000 per cent (Nelemans, Yungelson & Portegies Zwart 2004). We assume a density ratio between the thin and thick disc population of cataclysmic variables of 1 to 56 (Groot et al., in prep.). We randomly populate the model Galaxy according to the space density distribution and keep only the objects that are in the field-of-view of the Sky2Night survey. We then estimate if each object would have been detected in the Sky2Night project if a dwarf nova outburst occurs. For this, we use the relation $M_V = 5.92 - 0.383P$, with P as the orbital period (Warner 1987), and assume that $V - R = 0$ at peak. We randomly draw periods from a sample of periods as found in CRTS (see Coppejans et al. 2014). With this simulation and eight detected dwarf novae, we derive a local dwarf nova volumetric rate of $4.6^{4.7}_{-2.4} \times 10^{-8}\,d^{-1}pc^{-3}$. As this rate is the combination of a space density and an outburst frequency, we can compare our result to measurements of either of these, which is illustrated in Fig. 5. This shows that our finding is consistent with the combination of

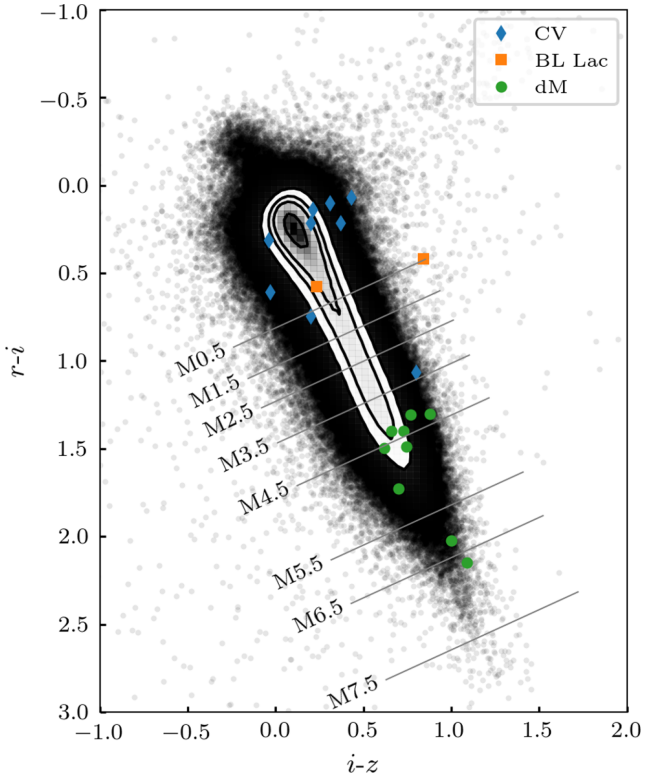

Figure 6. The Pan-STARRS colours of unresolved counterparts of transients. The black dots and contours show all point-sources in the Sky2Night area.

the measured space density of $2.3^{9.0}_{-1.4} \times 10^{-6}\,pc^{-3}$ (approximated 95 per cent interval, Pretorius & Knigge 2012) and, at the same time, an average outburst frequency of dwarf novae of $20^{+15}_{-8} \times 10^{-3}\,d^{-1}$ (calculated from the sample of Coppejans et al. 2014).

5.1.3 *Stellar flares*

In order to make a more direct comparison with flare rates from other surveys, we calculate the average flare duty cycle per M-dwarf spectral type. First, we use *ri* and *iz* colours from Pan-STARRS (Flewelling et al. 2016) to determine the number of stars per spectral type in the Sky2Night area, see Fig. 6. To calculate the average flare duty cycle, we divide the number of flare epochs by the total number of observations per spectral type, see Fig. 7.

This shows that, on average, the late type M-dwarfs are more active, which confirms earlier findings by Kowalski et al. (2009) and Hilton et al. (2010) (both with SDSS data), also plotted in Fig. 7. All findings show a similar trend, but the absolute numbers are three orders of magnitude off. This is the result of different flare selection criteria: Kowalski et al. (2009) selected flares with $\Delta u >$ 0.7 in Stripe 82 data, and Hilton et al. (2010) use Balmer emission lines in SDSS spectra to identify flares, but these lines can be a sign of persistent chromospheric activity as well. The main difference is that the contrast in the u-band and of emission lines of flares is much higher than in the R-band. Models by Davenport et al. (2012) can be used to convert ΔR to Δu (assuming $r = R$); a flare of $\Delta R = 0.6$ on an M4 star corresponds to a Δu of 4 magnitudes. This makes all flares which we found brighter than at least 99 per cent of the flares found in Kowalski et al. (2009). This explains the large difference in observed rates: Kowalski et al. (2009) reported an observed rate

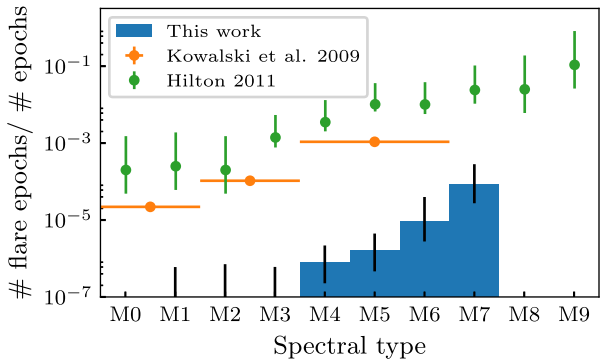

Figure 7. The fraction of time M-stars are in outburst for different spectral types. This is calculated by counting the number of flares per spectral type and dividing by the total number of M-stars of that spectral type in the S2N field, see Fig. 6. The error bars indicate the Poisson uncertainties only.

of 48 flaresdeg^{-2} d^{-1}, a factor 2600 higher than our results (see Table 3). This is also consistent with the difference between the duration and flare energy compared to the relation plotted in fig. 5.8 of Hilton (2011). The flares found in the Sky2night project are all at the high-energy, long-decay time end of the distributions.

We compare the rate of flares with the 38 M-flares found in the entire iPTF survey by Ho et al. (2018). Using their estimate for $E_A = 22146$ deg^2 d, the rate of such flares is $\mathcal{R} = 17^{+6}_{-5} \times 10^{-4}$deg^{-2} d^{-1}. Ho et al. (2018) rejected any transients with a stellar counterpart in the PTF reference images, so we compare it to the rate of flares with a counterpart fainter than the detection limit: $35^{+64}_{-26} \times 10^{-4}$deg^{-2} d^{-1}(Table 3). The rate from Sky2Night is slightly higher but consistent with the flare rate by Ho et al. (2018).

5.2 Upper limit for fast optical transients

Since no unclassified fast optical transients were found in our search, we have calculated upper limits for the rate of fast optical transients visible for 4 h and 1 d (see Section 4.3 and Tables 3). We compare our upper limits to upper limits determined by other searches for fast optical transients, see Fig. 8. Our result is most similar to the upper limit set by Cowperthwaite et al. (2018): 0.07deg^{-2} d^{-1} down to 22.5 in *i*-band at a time scale of 3 h. The Sky2Night upper limit is a factor of ≈15 lower, but at magnitude 19.7, 2.8 magnitudes lower. The Sky2night upper limit for 1 d transients is a factor 2.5 times deeper than the limit set by Berger et al. (2013) using *g*- and *r*-band data from Pan-STARRS. However, the PanSTARRS limiting magnitude is again 2.8 magnitudes deeper than the Sky2night search, making the Pan-STARRS upper limit slightly more constraining.

A lower limit to the rate of fast optical transients is set by GRB afterglows. During the entire duration of PTF, one GRB afterglow was found as a fast optical transient: PTF14yb (Cenko et al. 2015). The transient was bright enough to be detected by PTF for a total of 5 h. Ho et al. (2018) did an archival search of all PTF transients and did not find any new fast optical transients besides flaring M-dwarfs. Given this one event, they calculated a rate for extragalactic fast optical transients (peak $m \leq 18$ and fade by Δmag > 2 in $\Delta t = 3$ h) of $\mathcal{R} = 4.5^{+17.8}_{-4.4} \times 10^{-5}$deg^{-2} d^{-1} (see also Cenko et al. 2015). This indicates that the limit set by the Sky2Night survey is approximately two orders of magnitude above the rate of extragalactic fast optical transients.

5.3 False positives in the search for kilonovae

The aLIGO/aVirgo detectors are scheduled for another observing run, starting in early 2019 ('O3"). The estimated distance horizon to detect BNS mergers is 65–120 Mpc, and the expected number of BNS detections is 1–50 events (Abbott et al. 2016). Systematic follow-up of all BNS gravitational wave events allows us to study kilonovae in more detail using spectroscopy and also determine the characteristics of the population of kilonovae. In order to do this, optical survey telescopes need to quickly identify the kilonova counterpart in an area of 120–180 deg^2 (Abbott et al. 2016). This will be more challenging than the search for the optical counterpart to GW170817, AT2017gfo, which was well-localized (40 deg^2), nearby (≈40 Mpc) and bright ($r \approx 17$ mag at peak). For nearby kilonovae, a galaxy-targeted survey is more efficient than surveying the entire aLIGO/aVirgo error-box (e.g. Gehrels et al. 2016). However, because aLIGO/aVirgo will be more sensitive, the majority of the BNS events will be more distant and thus fainter. In those cases, a Galaxy-targeted search is less viable as the nearby Galaxy census is less complete at higher distances (e.g. Kulkarni, Perley & Miller 2018). Instead, an untargeted search will be needed to locate kilonova counterparts. The different search strategy, but also the fainter target, means that the number of false positives can become problematic. False positives delay the identification of the true kilonova counterpart and ruling them out requires valuable follow-up resources. In this section, we use results from the Sky2Night project to assess how problematic false positives are in a monochromatic kilonova search, and determine the best way to recognize false positives.

The Sky2Night survey area of the 407deg^2, two to three times the typical 'O3" errorbox of aLIGO/aVirgo, contained a total of 1012 transient candidates. Most of these were associated with variable stars or bad subtractions of stars (873 out of 1012). These can be identified by the presence of a star in the reference images (or other surveys). During the execution of Sky2Night, the identification of stellar counterparts was done by human inspection, but an automated procedure is easy to implement and is now standard in many transient identification pipelines (e.g. Miller et al. 2017). In addition, better image subtraction techniques such as ZOGY (Zackay, Ofek & Gal-Yam 2016) and also more advanced 'RealBogus' methods (e.g. Gieseke et al. 2017) have been developed. Moreover, the increase in available training data for the machine learning based 'RealBogus' also improves the identification of real transients. Improvement of this processing step will reduce, in particular, false positives due to poor subtractions of images, and should especially help in removing any nuclear transients which are the result of a slight misalignment of images. If we reject any candidate with a point-source counterpart (888), which is an improper subtraction (26), which is located at the core of a galaxy (48), or is moving (35), only 15 real transients remain out of the 1012 initial candidates.

The remaining 15 transients either have a nearby galaxy as a counterpart or no counterpart at all in the PTF images. The time evolution of a transient is one of the most discriminating properties of a transient, and Sky2Night light curves probe the evolution on time-scales of 2 h to 8 d. If we compare the light curves of the flare stars with that of a kilonova, we can easily tell them apart as flares evolve much faster than any kilonova. On the other hand, kilonovae evolve significantly in a timespan of 8 d, while supernovae light curves generally change only slightly in an 8-d timespan. They are therefore also easy to distinguish with an 8-d light curve. However, the two outbursting CVs with a faint quiescent counterpart (PTF10aaqc and PTF10aaqt) evolve on a similar time-

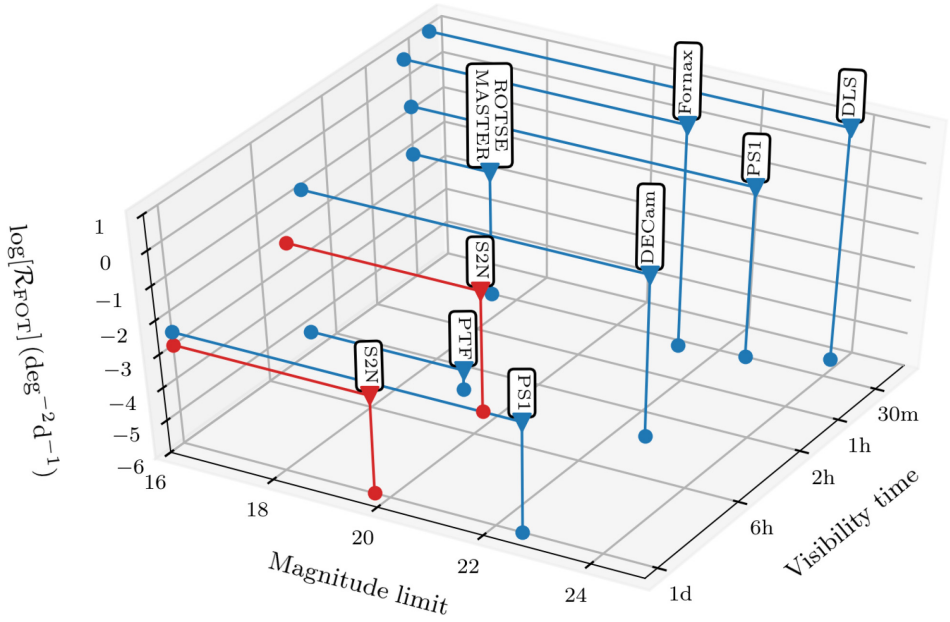

Figure 8. Upper limit to the rate of fast optical transient versus time-scale and limiting magnitude (adapted from Berger et al. 2013). The limits set by this work are shown in red and are labelled 'S2N'. Upper limits by other surveys are indicated in blue; Deep Lensing Survey (DLS, Becker et al. 2004), ROTSE/MASTER (Rykoff et al. 2005; Lipunov et al. 2007), Fornax Survey (Fornax, Rau et al. 2008), Pan-STARRS Berger et al. ('PS1', 2013), survey by the DECam (DECam, Cowperthwaite et al. 2018), and a search of all PTF data (PTF, Ho et al. 2018).

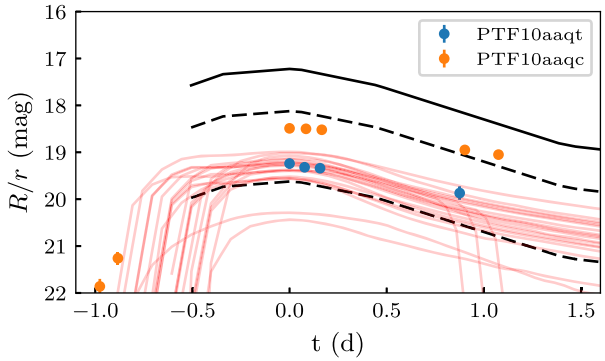

Figure 9. A comparison between the light curves of the DN detected in the Sky2Night project and kilonova light curves. All light curves have been shifted such that their peak occurs at t = 0. The black line indicates the best fit light curve of AT2017gfo in *r*-band (Villar et al. 2017). The dashed and dotted lines show this light curve for distances of 60 Mpc and 120 Mpc, the expected range of aLIGO/aVirgo during 'O3'. The red lines show kilonovae models by Kasen et al. (2017) at a distance of 120 Mpc.

scale as kilonovae, as shown in Fig. 9. The rise time is <1 d and the decay time-scale is ≈1 mag d^{-1}. Although the dwarf novae in our example rise and decay slightly slower, the difference will be almost impossible to detect with just a few epochs of data. With only this short span of data and if no additional information, such as historic light curves that may identify previous dwarf nova outburst, making the distinction between a kilonova and a young dwarf nova will be problematic. To distinguish a kilonova and a dwarf nova we need to rely on additional information (if no counterpart is detected). In the case of PTF10aaqc and PTF10aaqt, PTF detected previous outbursts, which confirmed the dwarf nova nature of the transients.

With the complete light curves, we have been able to reject all transients as kilonova candidates. However, the goal of kilonova searches is to identify the kilonova as fast as possible so it can be targeted for follow-up observations. Therefore, we should consider the question: can we reject all transients with only 1 d of data? In that case, the transient light curves contain only a few epochs, and the time-span is only a few hours. Next to dwarf novae now also supernovae become problematic, depending on the time since the merger for the kilonova searches. Supernovae do not evolve significantly in an 8-h timespan, and therefore can be confused with a kilonova at peak when it is relatively constant (approximately 10–24 h after the merger, ≈24 h for AT2017gfo). This ambiguity can be solved if the host redshift is known, and the absolute magnitude of the transient can be calculated. However, this information is not always available at the moment the transient is first detected.

We conclude that the rapid (within 24 h) unique identification of (faint) kilonovae using only a monochromatic transient light curve is difficult due to false positives. This is especially a problem if no counterpart can be identified and no recent pre-merger images are available. The latter issue can be solved by monitoring the entire (available) sky every night. This ensures that all repeating Galactic dwarf novae will be discovered and also that slowly evolving supernovae can be identified and can be discarded as kilonovae. However, this is resource intensive and not always possible (due to weather) and would still leave infrequent outbursting dwarf novae and young supernovae as potential false positives. The second solution is to obtain additional information by performing a two-band survey search to obtain instantaneous colours (e.g. $g - r$) of all transients. According to simulations kilonovae rapidly become redder within the first few days. This was also seen for AT2017gfo were the $g - r$ colour changed by ≈0.8 mag d^{-1}. This means that within 8 hours it became redder by ≈0.3 mag which should be easily detectable, even at low signal-to-noise ratios.

Cowperthwaite et al. (2018) have explored the colour solution and performed an empirical study of false positives with DECam (mounted at the 4 m Blanco telescope). They surveyed an area of

56 deg^2 for 5 nights at a cadence of 3 h with $i-z$ colour information. Out of the 929 transient candidates they found, all but 21 can be rejected as a potential kilonova using static colour information. A further inspection of the luminosity and colour evolution is enough to reject all of them as kilonova candidates. Utsumi et al. (2018) empirically tested the number of false positives expected in searches for kilonovae with the Hyper-SuprimeCam installed on the 8.2 m Subaru telescope. They obtained two sets of i and z images separated by 6 d covering 64 deg^2, in which they discovered a total of 1744 transient candidates. They applied colour and variability cuts aimed at identifying kilonovae. They concluded that all supernovae and AGN can be rejected as kilonovae candidates. However, two transients remained satisfying the kilonova criteria: a flare on a M-dwarf or M-giant and a CV outbursts.

The conclusion is that the automatic rejection of all false positives without any additional follow-up is difficult. We have shown that high-cadence (2 h) survey alone is not sufficient to identify all transients. A combination of high cadence, multicolour light curves combined with historical information are needed to quickly identify transient found in gravitational wave follow-up. We note that the biggest colour change is between the extremes of the optical regime (faster decay with bluer colour). Therefore a colour such as ($u-z$) would have the highest diagnostic power when probing deep enough.

6 SUMMARY AND CONCLUSIONS

In this paper, we present a systematic, unbiased survey of intra-night transients. We used PTF to survey 407 deg^2 at a cadence of 2 h combined with large-scale, systematic follow up with the WHT telescope. We performed a thorough search for transients, both Galactic and extragalactic. Our search identified 35 transients: 8 type-Ia SN, 2 Core-collapse SN, 3 unknown SN, 10 outbursting CVs, 9 flaring M-stars and 3 AGN flares. For each of these types of transients, we have calculated an observed rate and confirmed these with simulations. We found no extragalactic fast optical transients and set a deeper upper limit on their observed rate.

Our main conclusions are that the rate of fast extragalactic transients is low, $\mathcal{R} < 37 \times 10^{-4}\mathrm{deg}^{-2}\,\mathrm{d}^{-1}$ and $\mathcal{R} < 9.3 \times 10^{-4}\mathrm{deg}^{-2}\,\mathrm{d}^{-1}$ for time-scales of 4 h and 1 d at a limiting magnitude of $R \approx 19.7$., and that they are not a source of confusion when searching for kilonovae. In addition, a monochromatic survey with a cadence of 2 hours, combined with longer time baseline information and static colour information is sufficient to be able to identify common transients such as flaring star, outbursting CVs and supernovae. Difficulties arise if the transients need to be identified within a single night, with only single-band photometry. Transient surveys that aim to identify kilonovae within the first night should observe with at least two bands, preferably widely separated in wavelength, multiple times per night.

ACKNOWLEDGEMENTS

We thank the referee for thoroughly reading the manuscript and providing us with useful comments and suggestions.

JvR acknowledges support from the Netherlands Research School of Astronomy (NOVA) and Foundation for Fundamental Research on Matter (FOM), and also the California Institute of Technology where a large part of this work was conducted.

Based on observations made with the William Herschel Telescope (WHT) operated on the island of La Palma by the Isaac Newton Group in the Spanish Observatorio del Roque de los Muchachos of the Instituto de Astrofísica de Canarias.

The Palomar Transient Factory project is a scientific collaboration between the California Institute of Technology, Columbia University, Las Cumbres Observatory, the Lawrence Berkeley National Laboratory, the National Energy Research Scientific Computing Center, the University of Oxford, and the Weizmann Institute of Science.

We thank E. Hsiao, N. Suzuki, and J. Botyanszki for the spectra of PTF10zbk and PTF10zdk observed with the Lick telescope. We thank I. Arcavi, D. Xu, and T. Matheson for observing PTF10zbk and PTF10zdk with the KPNO Mayall telescope. We thank E. Hsiao, N. Suzuki, J. Botyanszki, and B. Cenko for the LRIS spectra of PTF10zdk, PTF10aaho, and PTF10aaey.

This research has made use of the SIMBAD data base, operated at CDS, Strasbourg, France.

This research made use of Astropy, a community-developed core Python package for Astronomy (Astropy Collaboration et al. 2013)

Funding for the Sloan Digital Sky Survey IV has been provided by the Alfred P. Sloan Foundation, the U.S. Department of Energy Office of Science, and the Participating Institutions. SDSS-IV acknowledges support and resources from the Center for High-Performance Computing at the University of Utah. The SDSS web site is www.sdss.org. SDSS-IV is managed by the Astrophysical Research Consortium for the Participating Institutions of the SDSS Collaboration including the Brazilian Participation Group, the Carnegie Institution for Science, Carnegie Mellon University, the Chilean Participation Group, the French Participation Group, Harvard-Smithsonian Center for Astrophysics, Instituto de Astrofísica de Canarias, The Johns Hopkins University, Kavli Institute for the Physics and Mathematics of the Universe (IPMU) / University of Tokyo, Lawrence Berkeley National Laboratory, Leibniz Institut für Astrophysik Potsdam (AIP), Max-Planck-Institut für Astronomie (MPIA Heidelberg), Max-Planck-Institut für Astrophysik (MPA Garching), Max-Planck-Institut für Extraterrestrische Physik (MPE), National Astronomical Observatories of China, New Mexico State University, New York University, University of Notre Dame, Observatário Nacional / MCTI, The Ohio State University, Pennsylvania State University, Shanghai Astronomical Observatory, United Kingdom Participation Group, Universidad Nacional Autónoma de México, University of Arizona, University of Colorado Boulder, University of Oxford, University of Portsmouth, University of Utah, University of Virginia, University of Washington, University of Wisconsin, Vanderbilt University, and Yale University.

The Pan-STARRS1 Surveys (PS1) have been made possible through contributions of the Institute for Astronomy, the University of Hawaii, the Pan-STARRS Project Office, the Max-Planck Society and its participating institutes, the Max Planck Institute for Astronomy, Heidelberg and the Max Planck Institute for Extraterrestrial Physics, Garching, The Johns Hopkins University, Durham University, the University of Edinburgh, Queen's University Belfast, the Harvard-Smithsonian Center for Astrophysics, the Las Cumbres Observatory Global Telescope Network Incorporated, the National Central University of Taiwan, the Space Telescope Science Institute, the National Aeronautics and Space Administration under Grant No. NNX08AR22G issued through the Planetary Science Division of the NASA Science Mission Directorate, the National Science Foundation under Grant No. AST-1238877, the University of Maryland, and Eotvos Lorand University (ELTE).

This research made use of matplotlib, a Python library for publication quality graphics (Hunter 2007).

REFERENCES

Abazajian K. N. et al., 2009, ApJS, 182, 543
Abbott B. P. et al., 2016, Living Rev. Relat., 19, 1
Abbott B. P. et al., 2017a, Phys. Rev. Lett., 119, 161101
Abbott B. P. et al., 2017b, ApJ, 848, L12
Abbott B. P. et al., 2017c, ApJ, 848, L13
Acernese F. et al., 2015, Class. Quant. Grav., 32, 024001
Ackermann M. et al., 2015, ApJ, 807, 169
Adams S. M. et al., 2018, PASP, 130, 034202
Andreoni I. et al., 2017, PASA, 34, e069
Arcavi I. et al., 2010, The Astronomer's Telegram, 3027
Arcavi I. et al., 2017, Nature, 551, 64
Astropy Collaboration et al., 2013, A&A, 558, A33
Barbary K., 2014, sncosmo v0.4.2,
Barnes J., Kasen D., 2013, ApJ, 775, 18
Becker A. C. et al., 2004, ApJ, 611, 418
Benn C., Dee K., Agócs T., 2008, in Ground-based and Airborne Instrumentation for Astronomy II. Vol. 7014, ACAM; a new imager/spectrograph for the William Herschel Telescope, Proc. SPIE, p. 70146X
Berger E. et al., 2013, ApJ, 779, 18
Bertin E., Arnouts S., 1996, A&AS, 117, 393
Best W. M. J. et al., 2018, ApJS, 234, 1
Blondin S., Tonry J. L., 2007, ApJ, 666, 1024
Bloom J. S. et al., 2012, PASP, 124, 1175
Boksenberg A., 1985, Vistas in Astronomy, 28, 531
Brink H., Richards J. W., Poznanski D., Bloom J. S., Rice J., Negahban S., Wainwright M., 2013, MNRAS, 435, 1047
Cao Y., Nugent P. E., Kasliwal M. M., 2016, PASP, 128, 114502
Cenko S. B. et al., 2013, ApJ, 769, 130
Cenko S. B. et al., 2015, ApJ, 803, L24
Chambers K. C. et al., 2016, preprint (arXiv:1612.05560)
Condon J. J., Cotton W. D., Greisen E. W., Yin Q. F., Perley R. A., Taylor G. B., Broderick J. J., 1998, AJ, 115, 1693
Coppejans D. L. et al., 2014, MNRAS, 437, 510
Coulter D. A. et al., 2017, Science, 358, 1556
Cowperthwaite P. S. et al., 2017, ApJ, 848, L17
Cowperthwaite P.S. et al., 2018, ApJ, 858:18
Davenport J. R. A., Becker A. C., Kowalski A. F., Hawley S. L., Schmidt S. J., Hilton E. J., Sesar B., Cutri R., 2012, ApJ, 748, 58
Drake A. J. et al., 2009, ApJ, 696, 870
Drake A. J. et al., 2010a, Central Bureau Electronic Telegrams, 2601
Drake A. J. et al., 2010b, The Astronomer's Telegram, 3081
Drake A. J. et al., 2014, MNRAS, 441, 1186
Drout M. R. et al., 2017, Science, 358, 1570
Díaz M. C. et al., 2017, ApJ, 848, L29
D'Abrusco R., Massaro F., Paggi A., Smith H. A., Masetti N., Landoni M., Tosti G., 2014, ApJS, 215, 14
Evans P. A. et al., 2017, Science, 358, 1565
Filippenko A. V., 1997, ARA&A, 35, 309
Filippenko A. V. et al., 1992a, AJ, 104, 1543
Filippenko A. V. et al., 1992b, ApJ, 384, L15
Flewelling H. A. et al., 2016, preprint (arXiv:1612.05243)
Fong W., Berger E., Margutti R., Zauderer B. A., 2015, ApJ, 815, 102
Frohmaier C., Sullivan M., Nugent P. E., Goldstein D. A., DeRose J., 2017, ApJS, 230, 4
Gehrels N., 1986, ApJ, 303, 336
Gehrels N., Cannizzo J. K., Kanner J., Kasliwal M. M., Nissanke S., Singer L. P., 2016, ApJ, 820, 136
Gershberg R. E., 1972, Ap&SS, 19, 75
Gezari S. et al., 2017, ApJ, 835, 144
Gieseke F. et al., 2017, MNRAS, 472, 3101
Gilliland R. L., Nugent P. E., Phillips M. M., 1999, ApJ, 521, 30
Graur O. et al., 2014, ApJ, 783, 28
Guy J. et al., 2007, A&A, 466, 11
Harrison T. E., Johnson J. J., McArthur B. E., Benedict G. F., Szkody P., Howell S. B., Gelino D. M., 2004, AJ, 127, 460
Hawley S. L., Davenport J. R. A., Kowalski A. F., Wisniewski J. P., Hebb L., Deitrick R., Hilton E. J., 2014, ApJ, 797, 121
Hilton E. J., 2011, PhD thesis, University of Washington
Hilton E. J., West A. A., Hawley S. L., Kowalski A. F., 2010, AJ, 140, 1402
Ho A. Y. Q. et al., 2018, ApJ, 854, L13
Hsiao E. Y., Conley A., Howell D. A., Sullivan M., Pritchet C. J., Carlberg R. G., Nugent P. E., Phillips M. M., 2007, ApJ, 663, 1187
Huchra J. P. et al., 2012, Astrophys. J. Suppl. Ser., 199, 26
Hu L. et al., 2017, Science Bulletin, 62, 1433
Hunter J. D., 2007, Comput. Sci. Eng., 9, 90
Kasen D., Fernández R., Metzger B. D., 2015, MNRAS, 450, 1777
Kasen D., Metzger B., Barnes J., Quataert E., Ramirez-Ruiz E., 2017, Nature, 551, 80
Kasliwal M. M., 2011, PhD thesis, California Institute of Technology
Kasliwal M. M. et al., 2017, Science, 358, 1559
Kato T. et al., 2009, PASJ, 61, S395
Kowalski A. F., Hawley S. L., Hilton E. J., Becker A. C., West A. A., Bochanski J. J., Sesar B., 2009, AJ, 138, 633
Kowalski A. F., Hawley S. L., Holtzman J. A., Wisniewski J. P., Hilton E. J., 2010, ApJ, 714, L98
Kulkarni S. R., 2005, Modeling Supernova-like Explosions Associated with Gamma-ray Bursts with Short Durations
Kulkarni S. R., Perley D. A., Miller A. A., 2018, ApJ, 860, 22
Kulkarni S. R., Rau A., 2006, ApJ, 644, L63
Law N. M. et al., 2009, PASP, 121, 1395
LIGO Scientific Collaboration et al., 2015, Class. Quant. Grav., 32, 074001
Li L.-X., Paczyński B., 1998, ApJ, 507, L59
Lipunov V., Kornilov V., Gorbovskoy E., Lipunova G., Vlasenko D., Panchenko I., Tyurina N., Grinshpun V., 2018, New A, 63, 48
Lipunov V. M. et al., 2007, Astronomy Reports, 51, 1004
Li W. et al., 2011, MNRAS, 412, 1441
Maguire K. et al., 2012, MNRAS, 426, 2359
Mandel K. S., Scolnic D. M., Shariff H., Foley R. J., Kirshner R. P., 2017, ApJ, 842, 93
Metzger B. D., Arcones A., Quataert E., Martínez-Pinedo G., 2010, MNRAS, 402, 2771
Metzger B. D., Fernández R., 2014, MNRAS, 441, 3444
Mickaelian A. M., Hovhannisyan L. R., Engels D., Hagen H.-J., Voges W., 2006, A&A, 449, 425
Miller A. A., Kulkarni M. K., Cao Y., Laher R. R., Masci F. J., Surace J. A., 2017, AJ, 153, 73
Nelemans G., Yungelson L. R., Portegies Zwart S. F., 2004, MNRAS, 349, 181
Oke J. B., Gunn J. E., 1982, PASP, 94, 586
Oke J. B. et al., 1995, PASP, 107, 375
Oliveira A. S., Rodrigues C. V., Cieslinski D., Jablonski F. J., Silva K. M. G., Almeida L. A., Rodríguez-Ardila A., Palhares M. S., 2017, AJ, 153, 144
Osaki Y., Kato T., 2013, PASJ, 65, 50
Pan Y.-C. et al., 2014, MNRAS, 438, 1391
Paturel G., Petit C., Prugniel P., Theureau G., Rousseau J., Brouty M., Dubois P., Cambrésy L., 2003, A&A, 412, 45
Pecaut M. J., Mamajek E. E., 2013, ApJS, 208, 9
Pian E. et al., 2017, Nature, 551, 67
Piran T., 1999, Phys. Rep., 314, 575
Pozanenko A. S. et al., 2018, ApJ, 852, L30
Pretorius M. L., Knigge C., 2012, MNRAS, 419, 1442
Rau A., Ofek E. O., Kulkarni S. R., Madore B. F., Pevunova O., Ajello M., 2008, ApJ, 682, 1205
Rau A. et al., 2009, PASP, 121, 1334
Roberts L. F., Kasen D., Lee W. H., Ramirez-Ruiz E., 2011, ApJ, 736, L21
Rosswog S., Feindt U., Korobkin O., Wu M.-R., Sollerman J., Goobar A., Martinez-Pinedo G., 2017, Class. Quant. Grav., 34, 104001
Rykoff E. S. et al., 2005, ApJ, 631, 1032
Schlegel D. J., Finkbeiner D. P., Davis M., 1998, ApJ, 500, 525
Schmidt S. J. et al., 2014, ApJ, 781, L24
Shappee B. J. et al., 2017, Science, 358, 1574

Silverberg S. M., Kowalski A. F., Davenport J. R. A., Wisniewski J. P., Hawley S. L., Hilton E. J., 2016, ApJ, 829, 129
Singer L. P. et al., 2015, ApJ, 806, 52
Smartt S. J. et al., 2017, Nature, 551, 75
Smith A. M. et al., 2011, MNRAS, 412, 1309
Szkody P., Everett M. E., Howell S. B., Landolt A. U., Bond H. E., Silva D. R., Vasquez-Soltero S., 2014, AJ, 148, 63
Tanaka M., Hotokezaka K., 2013, ApJ, 775, 113
Tanvir N. R. et al., 2017, ApJ, 848, L27
Taubenberger S., 2017, in Alsabti A., Murdin P., eds, Handbook of Supernovae, Springer, Cham, Switzerland
Troja E. et al., 2017, Nature, 551, 71
Utsumi Y. et al., 2017, PASJ, 69, 101
Utsumi Y. et al., 2018, PASJ, 70, 1
Valenti S. et al., 2017, ApJ, 848, L24
Vida K., Kővári Z., Pál A., Oláh K., Kriskovics L., 2017, ApJ, 841, 124
Villar V. A. et al., 2017, ApJ, 851, L21
Warner B., 1987, MNRAS, 227, 23
Warner B., 2003, Cataclysmic Variable Stars. Cambridge University Press, p. 592
Wittman D. M., et al., 2002, in Tyson J. A., Wolff S., eds, Proc. SPIEVol. 4836, Survey and Other Telescope Technologies and Discoveries. Deep lens survey, p. 73
Yaron O., Gal-Yam A., 2012, PASP, 124, 668
Zackay B., Ofek E. O., Gal-Yam A., 2016, ApJ, 830, 27

APPENDIX A: ADDITIONAL FIGURES AND TABLES

Table A1. The coordinates, the average extinction, and brightest stars of PTF fields observed during the project.

FieldID	RA (°)	Dec (°)	Ec. Lon. (°)	Ec. Lat. (°)	Gal. Lon. (°)	Gal. Lat. (°)	$E(B-V)$	Brightest star (mag)
3430	16.0396	16.875	21.2721	9.2741	127.306	−45.8887	0.045	5.68
3431	19.604	16.875	24.459	7.9678	132.161	−45.5128	0.078	3.71
3432	23.1683	16.875	27.6492	6.6942	136.916	−44.8742	0.089	3.71
3433	26.7327	16.875	30.8459	5.4573	141.528	−43.9839	0.053	5.21
3434	30.297	16.875	34.0516	4.261	145.96	−42.8563	0.061	5.21
3435	33.8614	16.875	37.2688	3.1092	150.189	−41.5079	0.098	5.89
3436	37.4257	16.875	40.4995	2.0057	154.198	−39.9567	0.454	6.05
3437	40.9901	16.875	43.7453	0.9542	157.982	−38.2211	0.1	5.32
3438	44.5545	16.875	47.0077	−0.0417	161.541	−36.319	0.224	5.32
3439	48.1188	16.875	50.2875	−0.9783	164.88	−34.2677	0.129	6.1
3440	51.6832	16.875	53.5855	−1.8524	168.01	−32.0832	0.123	6.26
3441	55.2475	16.875	56.9018	−2.6606	170.943	−29.78	0.221	6
3442	58.8119	16.875	60.2362	−3.3998	173.694	−27.3716	0.436	5.91
3531	16.2	19.125	22.3031	11.2882	127.294	−43.6335	0.04	4.77
3532	19.8	19.125	25.4973	9.9791	131.952	−43.26	0.054	4.77
3533	23.4	19.125	28.6931	8.7045	136.519	−42.6317	0.055	5.34
3534	27.0	19.125	31.8936	7.4682	140.956	−41.7586	0.059	5.21
3535	30.6	19.125	35.1015	6.2741	145.233	−40.6537	0.08	5.21
3536	34.2	19.125	38.3192	5.1263	149.324	−39.3323	0.136	5.28
3537	37.8	19.125	41.5487	4.0284	153.216	−37.8109	0.096	5.57
3538	41.4	19.125	44.7918	2.9841	156.9	−36.1066	0.085	5.17
3539	45.0	19.125	48.0498	1.9971	160.376	−34.2362	0.194	4.45
3540	48.6	19.125	51.3236	1.0707	163.647	−32.216	0.106	4.45
3541	52.2	19.125	54.614	0.2084	166.722	−30.0612	0.169	4.87
3542	55.8	19.125	57.921	−0.5867	169.611	−27.7861	0.405	5.67
3543	59.4	19.125	61.2446	−1.3117	172.326	−25.4034	0.321	5.62
3631	16.5306	21.375	23.4947	13.2383	127.489	−41.3668	0.041	4.5
3632	20.2041	21.375	26.7269	11.9154	132.004	−40.9786	0.048	4.77
3633	23.8775	21.375	29.9592	10.6295	136.434	−40.3384	0.07	5.34
3634	27.551	21.375	33.1947	9.3848	140.743	−39.4557	0.07	4.8
3635	31.2245	21.375	36.4363	8.1853	144.9	−38.3429	0.126	4.8
3636	34.898	21.375	39.6865	7.0349	148.883	−37.0148	0.101	5.04
3637	38.5714	21.375	42.9474	5.9376	152.679	−35.487	0.135	5.47
3638	42.2449	21.375	46.2206	4.897	156.279	−33.776	0.342	5.17
3639	45.9184	21.375	49.5076	3.9168	159.683	−31.898	0.432	4.45
3640	49.5918	21.375	52.8094	3.0004	162.892	−29.8688	0.333	4.45
3641	53.2653	21.375	56.1264	2.1513	165.913	−27.7033	0.185	5.22
3642	56.9388	21.375	59.4589	1.3726	168.757	−25.4154	0.191	5.43
3729	16.701	23.625	24.5571	15.2451	127.469	−39.1113	0.043	4.5
3730	20.4124	23.625	27.7929	13.9204	131.812	−38.7253	0.065	4.79
3731	24.1237	23.625	31.0272	12.6345	136.076	−38.0941	0.1	6.24
3732	27.835	23.625	34.263	11.3916	140.229	−37.2265	0.119	4.8
3733	31.5464	23.625	37.5033	10.1956	144.245	−36.1341	0.084	4.8
3734	35.2577	23.625	40.7507	9.0505	148.101	−34.8302	0.09	5.04

Table A1 *– continued*

FieldID	RA (°)	Dec (°)	Ec. Lon. (°)	Ec. Lat. (°)	Gal. Lon. (°)	Gal. Lat. (°)	$E(B-V)$	Brightest star (mag)
3735	38.9691	23.625	44.0071	7.9601	151.786	−33.3295	0.134	5.47
3736	42.6804	23.625	47.2745	6.9281	155.289	−31.6474	0.207	5.17
3737	46.3918	23.625	50.5542	5.958	158.61	−29.799	0.141	5.17
3738	50.1031	23.625	53.847	5.0533	161.748	−27.7994	0.212	5.46
3739	53.8144	23.625	57.1536	4.2172	164.71	−25.6627	0.22	3.6
3826	17.0526	25.875	25.7913	17.1841	127.647	−36.8431	0.086	4.75
3827	20.8421	25.875	29.0625	15.8464	131.867	−36.4421	0.119	4.75
3828	24.6316	25.875	32.3304	14.5504	136.012	−35.7978	0.1	6.25
3829	28.4211	25.875	35.5986	13.3004	140.052	−34.9189	0.116	4.8
3830	32.2105	25.875	38.87	12.1004	143.961	−33.8163	0.063	4.8
3831	36.0	25.875	42.1473	10.9545	147.72	−32.503	0.088	5.02
3832	39.7895	25.875	45.4327	9.8665	151.315	−30.9931	0.153	3.58
3833	43.5789	25.875	48.7279	8.8402	154.739	−29.3015	0.096	3.58
3834	47.3684	25.875	52.0342	7.8791	157.988	−27.443	0.197	5.46
3835	51.1579	25.875	55.3527	6.9866	161.063	−25.432	0.152	5.64

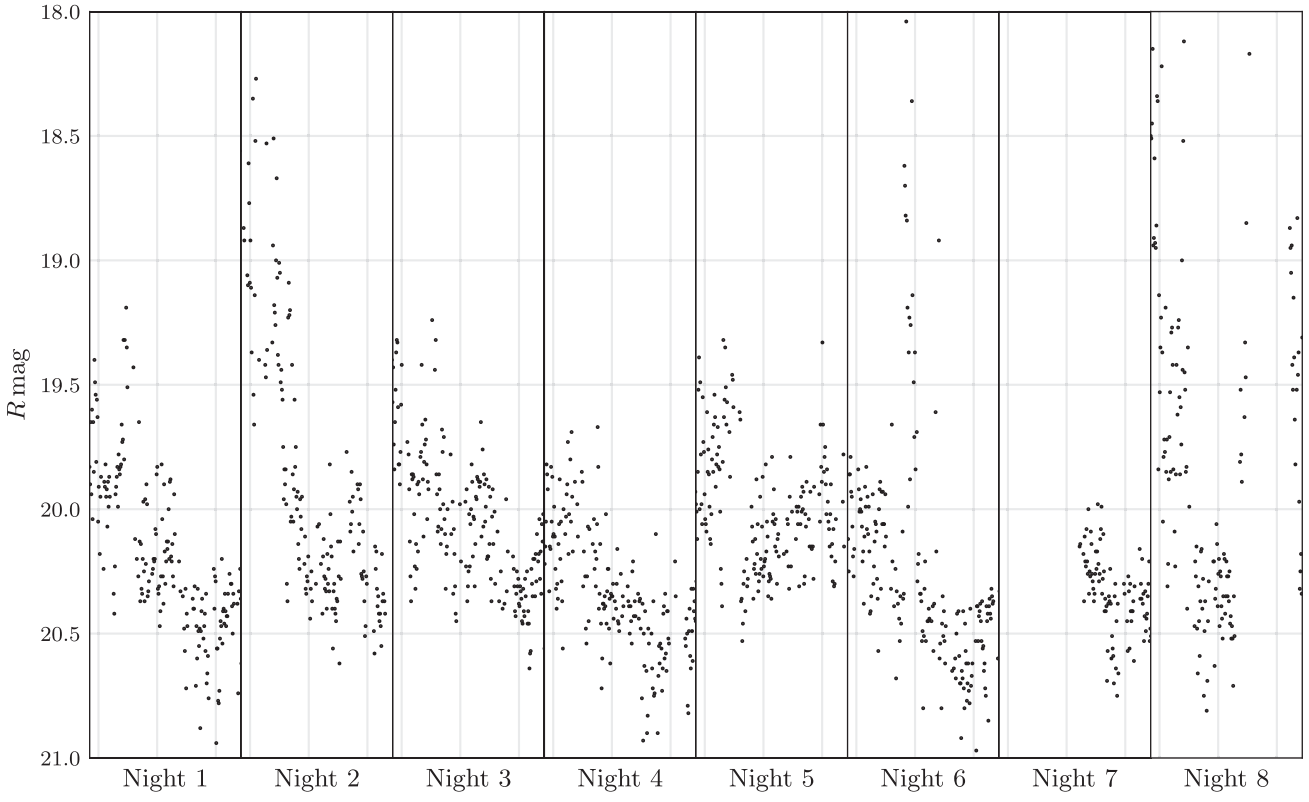

Figure A1. The limiting magnitude of the P48 images as function of time. Night 1 starts on MJD 55501.08.

Table A2. Overview of the weather conditions during the observations. The time inbetween astronomical twilight was approximately 12.3 h for both PTF and WHT.

		Night 1	Night 2	Night 3	Night 4	Night 5	Night 6	Night 7	Night 8
PTF	time lost (h)	0.6	3.7	0.1	0.2	0.7	0.4	3.7	6.0
	seeing (″)	2.5-3.5	3.0	3.0	2.5	2.0-3.5	2.0	3.0	2.5-3.5
	cloud conditions	good	good	good	ok	ok	ok	bad/ok	bad
WHT	time lost (h)	0	3.0	10.3	0	0	0	6.7	
	seeing (″)	1.5-2.5	1.5-3.0	2.5	2.5	1.5-2.5	1.0	2-3	
	cloud conditions	good	ok-bad	bad	good	good	good	good	

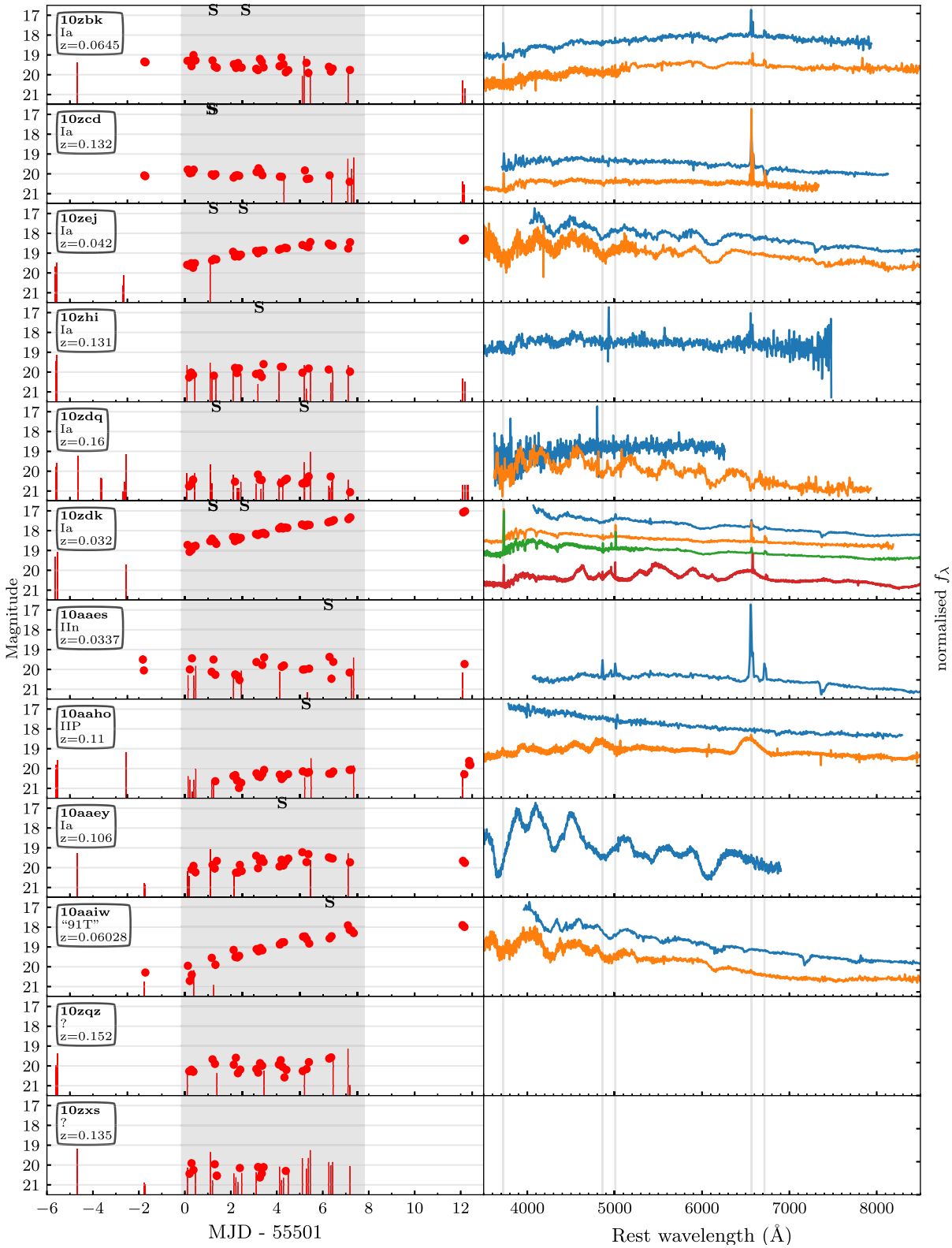

Figure A2. Light curves and spectra of all supernovae found during the project. The grey-shaded area indicates the duration of the Sky2Night project. The spectra are normalized to the median and offset by 1, from high to low according to time obtained and also coloured according to the time of observation from blue, yellow, green and red. The grey lines indicate common spectral lines: H α, H β, O II, O III, and S II. Note that some improperly subtracted telluric lines are visible in the spectra of PTF10zhi (4940 Å) and for PTF10zdq (4800 Å). The last spectrum of PTF10zdk was taken 37 d after the start of the Sky2Night project (MJD 55538).

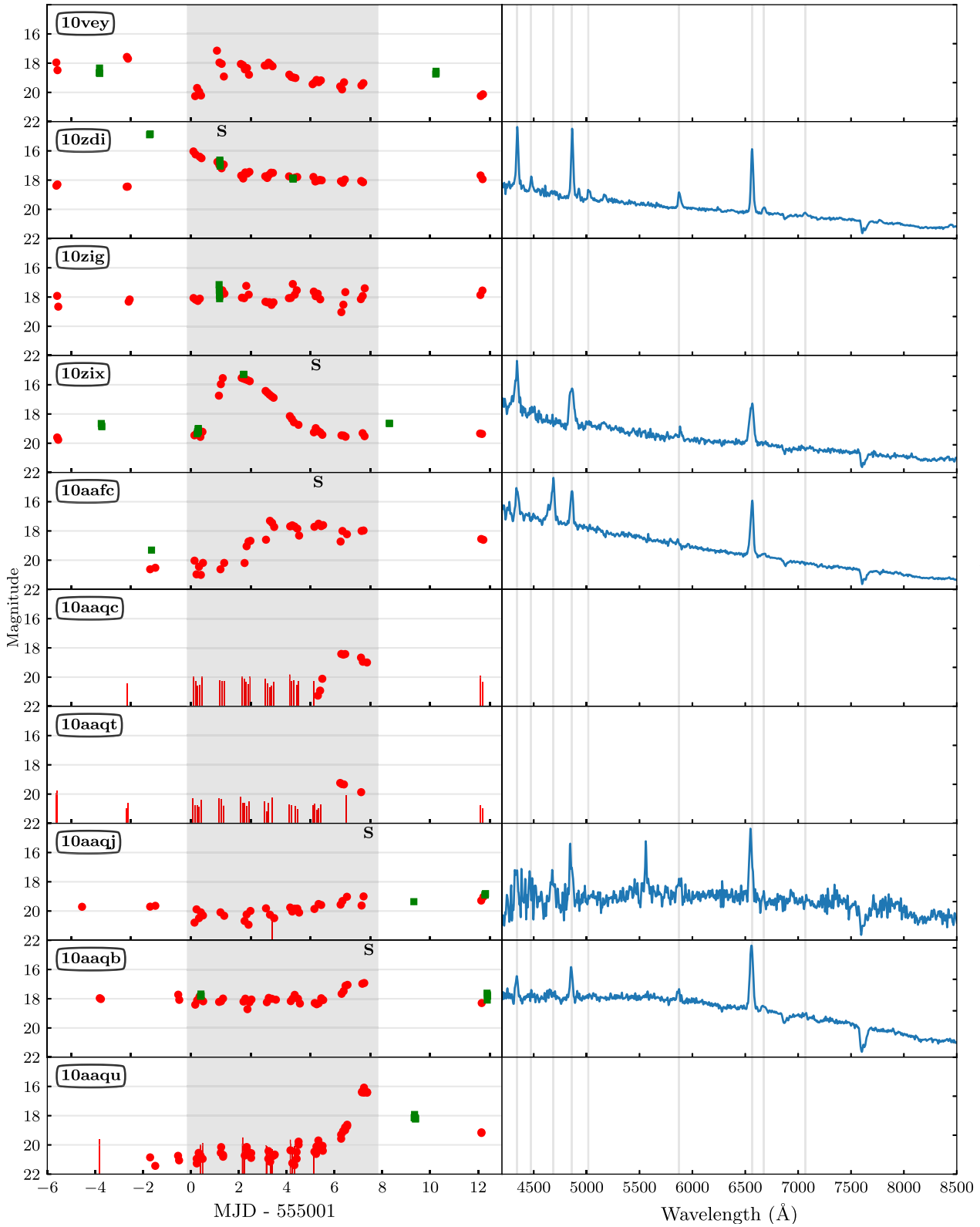

Figure A3. Light curves and spectra of all cataclysmic variables found during the project. The red dots indicate PTF photometry and vertical red lines indicate upper limits (*R* filter), green squares indicate CRTS photometry (no filter). The grey-shaded area indicates the duration of the Sky2Night project. All spectra were obtained with ACAM and normalized to the mean value. Grey lines show the Balmer lines, He I, and He II lines. The emission feature at 5577 Å in the spectrum of PTF10aaqj is caused by a telluric line.

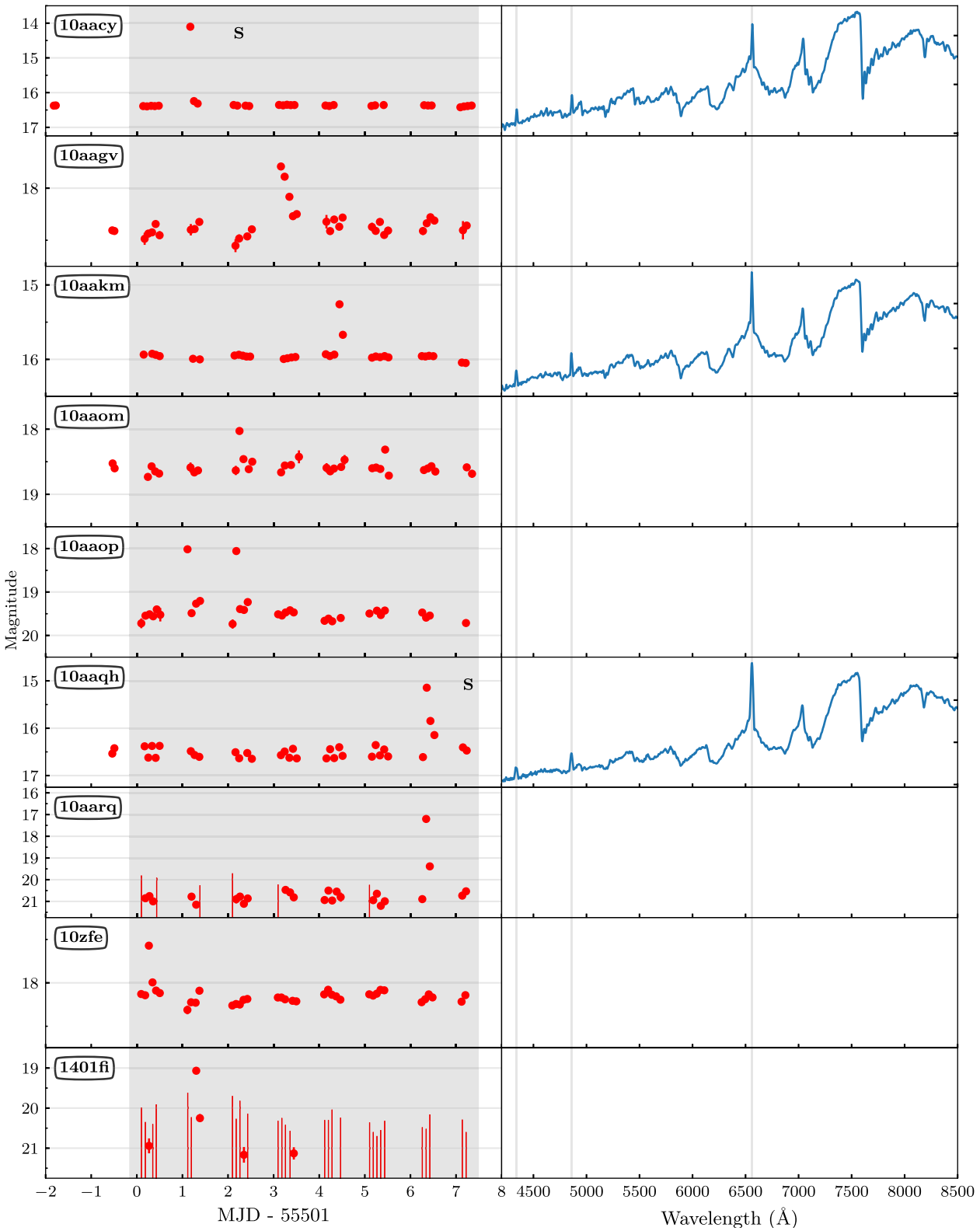

Figure A4. light curves and spectra of all stellar flares. The red dots indicate PTF photometry (*R* filter), vertical lines indicate upper limits. The grey shaded area indicates the duration of the Sky2Night project. All spectra were obtained with ACAM and normalized to the mean value. Grey lines show the Balmer lines.

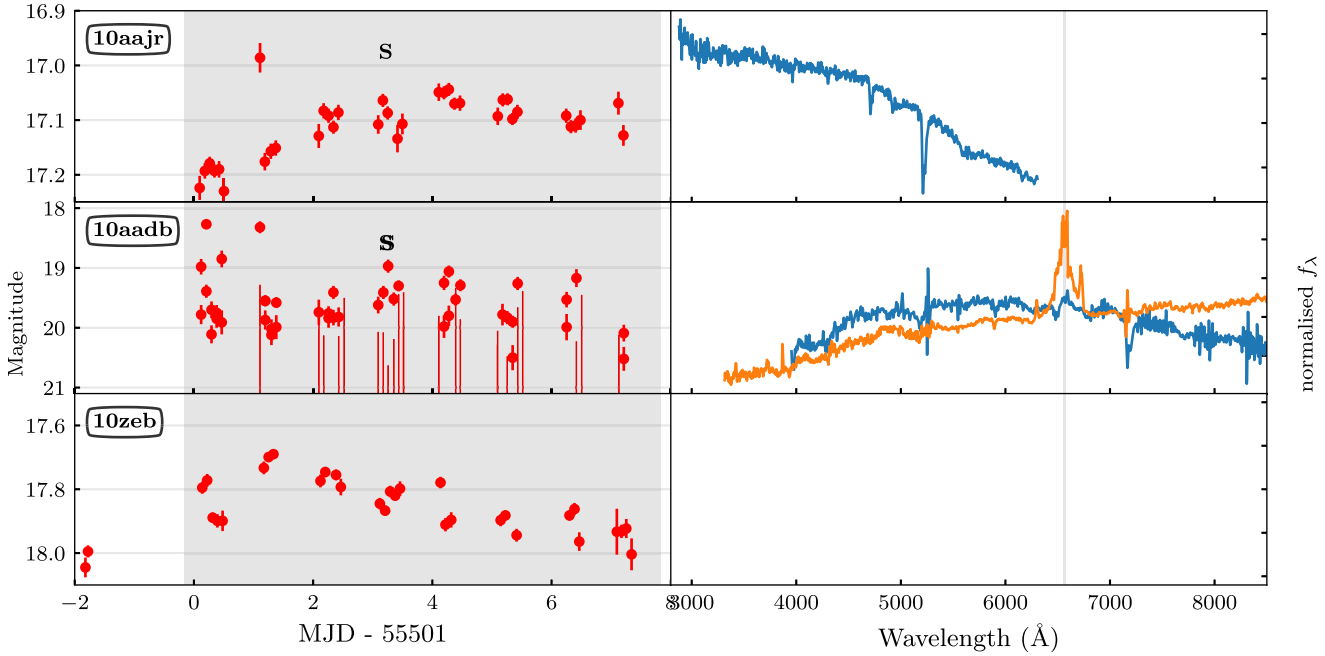

Figure A5. The light curves and spectra of flaring AGN. The red dots indicate PTF photometry (*R* filter), vertical lines indicate upper limits. The grey-shaded area indicates the duration of the Sky2Night project. The light curve for extended object PTF10aadb is made using the difference images, the other two light curves (two QSOs) are made without subtraction of the reference image. Spectra were obtained with ACAM and LRIS and normalized to the mean value. The DBSP spectrum of PTF10aadb (yellow) was taken 28 d after the start of the project while the ACAM spectrum (blue) was obtained at day 3 of the project. The grey line indicates the H α line.

Table A3. Number of observations of each field. Night 1 starts at MJD 55501.08.

FieldID	Night 1	Night 2	Night 3	Night 4	Night 5	Night 6	Night 7	Night 8	Total
3430	4	3	4	4	3	4	2	4	28
3431	4	3	5	5	3	4	2	4	30
3432	4	3	5	5	3	4	3	4	31
3433	5	3	4	5	3	3	3	4	30
3434	5	3	5	5	3	4	3	4	32
3435	5	3	5	5	4	5	3	4	34
3436	5	4	5	5	3	4	3	3	32
3437	5	3	5	4	3	5	3	3	31
3438	5	3	4	5	3	5	3	3	31
3439	5	3	5	5	4	5	3	3	33
3440	5	3	5	5	4	5	4	3	34
3441	4	3	5	5	5	5	4	3	34
3442	5	3	5	4	5	5	4	3	34
3531	5	5	4	5	5	4	2	3	33
3532	5	2	4	5	5	4	3	3	31
3533	4	3	4	5	5	4	3	3	31
3534	5	4	4	5	5	4	3	3	33
3535	5	4	5	5	5	5	3	4	36
3536	4	4	4	5	5	5	3	4	34
3537	5	4	5	5	5	5	3	4	36
3538	4	4	5	6	6	5	3	3	36
3539	5	3	5	5	4	5	4	3	34
3540	5	3	5	5	5	5	4	3	35
3541	5	3	5	5	5	5	4	3	35
3542	4	3	5	5	5	6	4	3	35
3543	4	3	5	5	5	5	4	2	33
3631	5	3	5	5	4	4	2	2	30
3632	5	4	5	5	4	4	3	3	33
3633	5	4	5	5	3	5	3	2	32
3634	5	2	5	5	5	5	3	2	32
3635	5	4	5	5	4	5	3	2	33

Table A3 – *continued*

FieldID	Night 1	Night 2	Night 3	Night 4	Night 5	Night 6	Night 7	Night 8	Total
3636	6	3	5	6	5	5	3	1	34
3637	5	4	5	5	5	5	3	3	35
3638	5	2	5	6	5	5	4	3	35
3639	5	3	5	5	5	4	4	2	33
3640	5	3	5	5	5	5	4	2	34
3641	5	3	5	4	5	5	4	2	33
3642	5	3	5	5	5	5	4	2	34
3729	5	3	5	5	5	4	3	2	32
3730	4	4	5	5	4	5	3	2	32
3731	5	4	5	4	5	5	4	1	33
3732	6	4	5	5	4	5	4	2	35
3733	6	4	5	5	5	5	4	2	36
3734	5	4	5	6	5	5	4	2	36
3735	5	4	6	6	5	5	4	1	36
3736	5	4	5	5	5	6	4	2	36
3737	5	3	5	5	5	5	4	2	34
3738	5	3	5	5	5	5	4	2	34
3739	5	3	5	5	5	5	4	2	34
3826	5	4	5	5	4	5	3	2	33
3827	5	4	5	4	5	5	3	2	33
3828	5	4	5	5	4	5	3	2	33
3829	6	4	5	5	5	5	3	2	35
3830	6	4	5	5	4	5	3	1	33
3831	5	4	6	6	5	6	3	2	37
3832	5	4	4	6	5	6	4	2	36
3833	5	3	5	5	5	6	4	2	35
3834	5	3	4	5	5	5	4	2	33
3835	5	3	5	5	5	5	4	2	34
median	5	3	5	5	5	5	3	2	34
total	290	200	287	296	266	285	199	151	1974

Table A4. Properties of the supernovae discovered during the Sky2Night project.

Name PTF ...	Type	Redshift (z)	peaktime (MJD-55501)
10zbk	Ia	0.0645(5)	-9 ± 3
10zcd	Ia	0.132(2)	-1.9 ± 1.8
10zej	Ia '91bg":	0.048(6)	11.5 ± 0.2
10zhi	Ia	0.128(5)	5.5 ± 1.4
10zdq	Ia	0.161(4)	0.3 ± 3.0
10zdk	Ia	0.033(1)	14.2 ± 0.1
10aaes	IIn	0.0337(1)	<-80
10aaho	IIP	0.108(4)	6.5 ± 0.4
10aaey	Ia	0.107(2)	8.4 ± 1.0
10aaiw	Ia '99T"	0.06028(2)	16.3 ± 0.3
10zxs	?	0.135(34)	
10zqz	?	0.152(38)	

Table A5. Properties of the CVs found during the Sky2Night project. The quiescence magnitude is given in *R* if it is detected in PTF images. If the counterpart is too faint, the PanSTARRS *r* magnitude is given.

Name PTF ...	Type	Quiescence (mag)	Δr (mag)
10vey	U Gem	$R = 20.5$	3.4
10zdi	U Gem	$R = 18.4$	2.4
10zig	SU UMa:/WZ Sge:	$r = 21.6$	5.5
10zix	U Gem	$R = 19.61$	3.9
10aafc	U Gem	$R = 20.17$	2.5
10aaqc	U Gem	$r = 22.0$	3.5
10aaqt	U Gem	$r = 23.0$	4.5
10aaqj	AM Her:	$R = 20.5$	1.0
10aaqb	U Gem	$R = 18.00$	1.2
10aaqu	U Gem	$R = 20.34$	4.3

Table A6. Properties of the flaring M-stars discovered during the Sky2Night project. PTF10aaop showed two outbursts in different nights.

Name PTF ...	Sp type	Quiescence *R* (mag)	ΔR (mag)	Time scale (h)	$\log E_R$ ($ergs^{-1}$)
10aacy	M4	16.4	2.3	0.5(1)	32.0
10aagv	M5	18.3	0.6	4.6(4)	32.0
10aakm	M4	15.9	0.6	1.6(1)	32.0
10aaom	M5	18.7	0.7	1.3(2)	31.4
10aaop	M7	19.5	1.5/1.5	<0.3/<0.6	30.0/30.4
10aaqh	M5	16.5	1.3	1.9(1)	32.1
10aarq	M6	20.7	3.5	0.8(1)	31.6
10zfe	M4	18.2	0.6	1.4(1)	32.0
1401fi	M4	21.3	2.2	1.2(2)	34.0

This paper has been typeset from a TEX/LATEX file prepared by the author.